

SANDIA REPORT

SAND2003-2204
Unlimited Release
Printed July 2003

A Brief Examination of Optical Tagging Technologies

Mark R. Ackermann, Paul A. Cahill, Timothy J. Drummond
and Jess P. Wilcoxon

Prepared by
Sandia National Laboratories
Albuquerque, New Mexico 87185 and Livermore, California 94550

Sandia is a multiprogram laboratory operated by Sandia Corporation,
a Lockheed Martin Company, for the United States Department of Energy's
National Nuclear Security Administration under Contract DE-AC04-94AL85000.

Approved for public release; further dissemination unlimited.



Issued by Sandia National Laboratories, operated for the United States Department of Energy by Sandia Corporation.

NOTICE: This report was prepared as an account of work sponsored by an agency of the United States Government. Neither the United States Government, nor any agency thereof, nor any of their employees, nor any of their contractors, subcontractors, or their employees, make any warranty, express or implied, or assume any legal liability or responsibility for the accuracy, completeness, or usefulness of any information, apparatus, product, or process disclosed, or represent that its use would not infringe privately owned rights. Reference herein to any specific commercial product, process, or service by trade name, trademark, manufacturer, or otherwise, does not necessarily constitute or imply its endorsement, recommendation, or favoring by the United States Government, any agency thereof, or any of their contractors or subcontractors. The views and opinions expressed herein do not necessarily state or reflect those of the United States Government, any agency thereof, or any of their contractors.

Printed in the United States of America. This report has been reproduced directly from the best available copy.

Available to DOE and DOE contractors from

U.S. Department of Energy
Office of Scientific and Technical Information
P.O. Box 62
Oak Ridge, TN 37831

Telephone: (865)576-8401
Facsimile: (865)576-5728
E-Mail: reports@adonis.osti.gov
Online ordering: <http://www.doe.gov/bridge>

Available to the public from

U.S. Department of Commerce
National Technical Information Service
5285 Port Royal Rd
Springfield, VA 22161

Telephone: (800)553-6847
Facsimile: (703)605-6900
E-Mail: orders@ntis.fedworld.gov
Online order: <http://www.ntis.gov/help/ordermethods.asp?loc=7-4-0#online>



SAND2003-2204
Unlimited Release
Printed July 2003

A Brief Examination of Optical Tagging Technologies

Mark R. Ackermann, Timothy J. Drummond and Jess P. Wilcoxon
Sandia National Laboratories, Department 5922
P.O. Box 5800, Albuquerque, NM 87185-1217

Paul A. Cahill
Aspecular Optics
10440 Stream Park Ct, Dayton OH 45458

Abstract

Presented within this report are the results of a brief examination of optical tagging technologies funded by the Laboratory Directed Research and Development (LDRD) program at Sandia National Laboratories. The work was performed during the summer months of 2002 with total funding of \$65k.

The intent of the project was to briefly examine a broad range of approaches to optical tagging concentrating on the wavelength range between ultraviolet (UV) and the short wavelength infrared (SWIR, $\lambda < 2\mu\text{m}$).

Tagging approaches considered include such things as simple combinations of reflective and absorptive materials closely spaced in wavelength to give a high contrast over a short range of wavelengths, rare-earth oxides in transparent binders to produce a narrow absorption line hyperspectral tag, and fluorescing materials such as phosphors, dyes and chemically precipitated particles.

One technical approach examined in slightly greater detail was the use of fluorescing nano particles of metals and semiconductor materials. The idea was to embed such nano particles in an oily film or transparent paint binder. When pumped with a SWIR laser such as that produced by laser diodes at $\lambda=1.54\mu\text{m}$, the particles would fluoresce at slightly longer wavelengths, thereby giving a unique signal.

While it is believed that optical tags are important for military, intelligence and even law enforcement applications, as a business area, tags do not appear to represent a high on return investment. Other government agencies frequently shop for existing or mature tag technologies but rarely are interested enough to pay for development of an untried technical approach. It was hoped that through a relatively small investment of laboratory R&D funds, enough technologies could be identified that a potential customers requirements could be met with a minimum of additional development work. Only time will tell if this proves to be correct.

This page intentionally left blank

Contents

1	Introduction	10
2	Background	11
2.1	The Problem	11
2.2	Target Tracking	11
2.3	Why Use Tags	12
2.4	Types of Tags	12
2.5	An Application	13
3	Technologies for Optical Tags	14
3.1	Focus on Commercial Technologies	14
3.2	Rare Earth Oxides for Hyperspectral Tags	15
3.3	UV Fluorescent or Hyperspectral Tags Based on Organic Compounds	25
3.3.1	Isolated Carbocyclic Ring Compounds	27
3.3.2	Condensed Carbocyclic Ring Compounds	27
3.3.3	Condensed Heterocyclic Ring Compounds	30
3.3.4	Compounds with isolated double bonds between heteroatoms	30
3.3.5	1, 2, 4-Triazol-3-ones and Related Compounds	33
3.3.6	Oligo(acetylenes)	33
3.3.7	Reflectivity of the Underlying Surface	35
3.3.8	Hosts for Deep UV Tags	36
3.3.9	Other UV Tags	36
4	Nano Particles and Opticules for use in Tags	40
4.1	A Theoretical Examination	40
4.1.1	Semiconductor Nanoclusters	41
4.1.2	Metallic Nanoclusters	42
4.1.3	Final Thoughts on Nanocluster Physics	44
4.2	Laboratory Investigation of Nano Particles	45
4.2.1	Nanocluster Sample Preparation	46
4.2.2	Factors affecting NIR and IR PL efficiency	48
4.2.3	Future Directions	53
5	Non Optical Tags	54
5.1	Magnetic Technologies	54
5.2	Chemical (Scent) Technologies	54
5.3	RF Harmonic Tags	54
5.4	Other New Technologies	55
5.5	Other Commercial Tagging Technologies	55
6	Summary	56

Figures

1	Low resolution transmission curve for Schott rare earth oxide doped glass Praseodymium S-8040 [2]	16
2	Low resolution transmission curve for Schott rare earth oxide doped glass Neodymium S-8041 [2]	17
3	Low resolution transmission curve for Schott rare earth oxide doped glass Samarium S-8042 [2]	17
4	Low resolution transmission curve for Schott rare earth oxide doped glass Europium S-8043 [2]	18
5	Low resolution transmission curve for Schott rare earth oxide doped glass Gadolinium S-8044 [2]	18
6	Low resolution transmission curve for Schott rare earth oxide doped glass Terbium S-8045 [2]	18
7	Low resolution transmission curve for Schott rare earth oxide doped glass Dysprosium S-8046 [2]	19
8	Low resolution transmission curve for Schott rare earth oxide doped glass Holmium S-8047 [2]	19
9	Low resolution transmission curve for Schott rare earth oxide doped glass Erbium S-8048 [2]	19
10	Low resolution transmission curve for Schott rare earth oxide doped glass Thulium S-8049 [2]	20
11	Low resolution transmission curve for Schott rare earth oxide doped glass Ytterbium S-8050 [2]	20
12	An example of complex spectral patterns in the near-IR that are available from mixtures of rare earth oxides. Spectrum of a glass optical filter designed containing several rare earth oxides to provide well defined absorbance features from $10,000\text{cm}^{-1}$ to $5,000\text{cm}^{-1}$. The filter glass contains 3.00 mole % Ho_2O_3 , 1.30 mole % Sm_2O_3 , 0.68 mole % Yb_2O_3 , and 0.47 mole % Nd_2O_3 . These concentrations were chosen to yield peak absorbances between 0.2 and 0.6 with 1.5mm thick filters [4,5]. Precise reference band positions are published in the Certificate for SRM 2035 [6].	21
13	Transmission and absorption spectrum for Holmium which has one of the most complex spectra of any rare earth material. These data are for Holmium oxide, 4%, in perchloric acid solution, 10% with a 1cm path length [7]. The data shown here reveal the details not visible in the Schott spectra (Figure 8). Details of the spectral peaks are given in Table 1.	22
14	Didymium's absorption spectrum is also complex. Note the strong absorption near $\lambda=580\text{-}600\text{nm}$ that removes the sodium flare in glassblowers' glasses [7]. Spectroscopic details of liquid samples are more pronounced in those for Schott glasses. Details of the spectral peaks are given in Table 2.	23

15	The Samarium absorption spectrum is characterized by one very strong peak with many weaker bands [7]. A pronounced spectral line occurs at about $\lambda=400\text{nm}$ which is most obvious in the absorption spectrum. Details of the spectral peaks are given in Table 3.	24
16	Luminescent Lumilass G9 emission (above) and excitation spectrum (below) [8]. Sumita claims exceptional brightness for this terbium based glass - ten times the efficiency of what they claim for the blue and red glasses.	25
17	Emission and excitation spectra for the europium based glass R7 [8].	26
18	Emission and excitation spectra of Lumilass B [8]. The emitting ion is probably europium +2.	26
19	Benzene, alkyl benzenes and alkoxybenzenes.	27
20	The ultraviolet spectrum of ethyl phenyl ether in ethanol at a concentration of 5×10^{-3} moles per liter consists of a single strong peak near $\lambda=270\text{nm}$ with weaker features in the $\lambda=300\text{-}350\text{nm}$ range. Line "C" is a 0.01cm path length, line "B" is 0.1cm path length and line "A" is for a 1.0cm path length [9]. The spectra of other alkoxy-substituted benzenes are similar.	28
21	Structures of condensed carbocyclic ring compounds.	28
22	The ultraviolet spectrum of 9,10-dimethylanthracene in absolute ethanol at a concentration of 1.152×10^{-5} moles per liter consists of a single strong peak near $\lambda=260\text{nm}$ with weaker features in the $\lambda=350\text{-}400\text{nm}$ range [9]. The spectra of other alkyl-substituted anthracenes are similar.	29
23	Structures of condensed heterocyclic ring compounds.	30
24	The ultraviolet spectrum of phenanthridine in the $\lambda=300\text{-}400\text{nm}$ region shows two especially narrow peaks at about $\lambda=328\text{nm}$ and $\lambda=343\text{nm}$. The full width at half maximum of these peaks is about 4nm - among the sharpest peaks of any organic molecule. The contrast ration in absorbance is not as high as other compounds discussed in this report, however. Other benzoquinolines show similar spectra. The spectra were taken in cyclohexene at the following concentrations: (1) 0.4886 grams/liter, (2) .04886 grams/liter, (3) lowest, 0.00489 grams/liter in a 1cm path length [9].	31
25	From left to right: N-(4-acetamidobenzenesulfonyl)-D-glucosylamine-2,3,4,6-tetraacetate), pentaaceyl-D-thiocgluconoamide, and tri(o-tolyl)phosphine oxide.	32
26	Example of a compound with a dip in absorbance in the UV that could be used as a high contrast tag by comparing reflectance at $\lambda \sim 230\text{nm}$ and $\lambda \sim 275\text{nm}$. The full width at half maximum is about 32nm. The contrast is about 14:1. Relatively few compounds show this degree of contrast in the deep UV. The concentration of the solute was 5×10^{-5} moles per liter (molecular weight 544.5) in ethanol with a 1cm path length [9].	32
27	Second example of a compound with a dip in absorbance in the UV that could be used as a high contrast tag by comparing reflectance at $\lambda \sim 230\text{nm}$ and $\lambda \sim 272\text{nm}$. The full width at half maximum is about 30nm. The contrast is about 53:1. Very few compounds show this degree of contrast in the deep UV. The concentration of the solute was 1×10^{-4} moles per liter (molecular weight 421.5) in ethanol with a 1cm path length [9].	33

28	4,4'-(1,2-ethanediyl)bis(2,4-dihydro-5-propyl-3H-1,2,4-triazol-3-one) and [(5-phenylmethyl)-2H-1,2,4-triazol-3-yl]ethanenitrile.	33
29	Ultraviolet spectrum of 4,4'-(1,2-Ethanediyl)bis(2,4-dihydro-5-propyl-3H-1,2,4-triazol-3-one) in ethanol at a concentration of 1.0mg/mL. The absorbance scale is arbitrary. The peak is at about $\lambda=225\text{nm}$ with a full width at half maximum of about 20nm. The spectra of other triazolones are similar [9]. . .	34
30	2-Chlorotrideca-3-ene-5,7,9,11-tetraen-1-ol.	35
31	Reflectivity data from Oriel "Book of Photon Tools". Most Retroreflectors require a thin metal reflector. Aluminum is an inexpensive and effective deep UV reflector. [10].	35
32	Reflectivity data from Oriel "Book of Photon Tools". Most Retroreflectors require a thin metal reflector. Aluminum is an inexpensive and effective deep UV reflector. [10].	36
33	A deep UV optical tag may require a transparent binder. Transparency in the deep UV requires that most or all of the binder be free of double bonds. Teflon®AF, a product of du Pont, is composed entirely of C-F, C-C, and C-O bonds and has good transparency in the deep UV. Unfortunately, it is a poor solvent for other materials and like Teflon®PTFE, is difficult to adhere to surfaces. Polymers such as poly(vinyl alcohol) but with crosslinks to form a tough material may be more effective.	38
34	Set-up for laser-line PL imaging of dilute solutions of nanoclusters.	46
35	Set-up for SWIR PL detection using an integrating sphere.	47
36	Set-up showing red PL from a CdS nanocluster sample illuminated with invisible, 365nm laser light and collected at a baffled detector of an integrating sphere.	47
37	Invisible UV illumination, 365nm, of CdS qdots of the same size but different interface chemistry shows blue, green, and red output from the dots, with high efficiency.	48
38	Invisible lamp illumination of a "nano-art-Qdot" face of CdSe (yellow in absorbance) on a paper towel glows intensely green. The Si CCD array also responds to the background ultraviolet illumination of the towel.	49
39	Absorbance spectra of nanosize PbS and the reference standard IR-26 both at 10^{-4}M . The ordinate is the fraction of the incident beam absorbed in 1cm.	49
40	TEM of nanosize SWIR emitting PbS whose spectra was shown in Figure 39.	50
41	HRTEM of nanosize red and SWIR emitting $D=3\text{nm}$ HgSe.	50
42	Absorbance and SWIR PL of HgSe in thf.	52

Tables

1	Spectral peaks for Holmium corresponding to those shown in Figure 13. . . .	17
2	Spectral peaks for Didymium corresponding to those shown in Figure 14. . .	20
3	Spectral peaks for Samarium corresponding to those shown in Figure 15. . .	21
4	Solvent Cut-off Wavelengths (Wavelengths where A=1 in 1 cm) for Pure Sol- vents [11].	37
5	Relative Q.E.s of Standard Dye vs Nanosize Semiconductors (excitation for $\lambda=514\text{nm}$ with a path length of 1cm, incident intensity was 320mW). . . .	51

1 Introduction

This report presents results of a brief examination of optical tagging technologies funded by the Laboratory Directed Research and Development (LDRD) program at Sandia National Laboratories. The work was conducted during the summer of 2002 with total funding of \$65k. The intent was to briefly examine a broad range of possible tagging technologies and to examine the performance of nano particle based tags in slightly more detail as work to understand their chemistry and physics could be leveraged from other programs. This report is not intended to be an extensive reference work. It simply reports results of a brief examination of possible technologies for optical tags.

In general, tags and tagging technologies represent a puzzling business area. Frequently we encounter government organizations interested in tags, or groups using tags but looking for better performance. Most often, the time scale for the need is short precluding any real development work. When proposed as a development activity, tags generally do not fair well as there exists at the time no urgent need, and in general, most agencies want fairly unique tags.

In an effort to partially address the recurring need for tagging technologies, we explored a wide variety of approaches for producing an optical tag ranging from materials which have unique characteristics at ultraviolet (UV) wavelengths, to materials which are more active at short wave infrared (SWIR) wavelengths.

2 Background

2.1 The Problem

The problem considered here is that of using an automated sensor system to both classify a specific type of targets out of a sea of potential targets and to identify individual specific targets out of a given class. For the human sensory perception system combined with the processing power of a human brain, this is in many cases an easy task. However, for artificial sensor systems, the task can be quite difficult.

Humans are amazingly adept at both classifying and identifying individual targets. A simple example of this is the ability of individuals to recognize the faces of other people, even out of a sizeable crowd. In many cases the ability persists even with only partial information such as a side view or an obstructed view. While artificial sensor systems can identify individuals once trained, the algorithms degrade rapidly with noise or partial information. The impact of target signal to background noise ratio is in most cases very pronounced with artificial sensors. While fusing the outputs of several sensors with different operating and sensing phenomenologies can greatly improve noise rejection, as a general rule, high noise environments are difficult for artificial sensors.

2.2 Target Tracking

When trying to track a target with artificial sensors, all the problems of finite detection probability and limited ability to operate in a noisy environment begin to compound. However, there are two types of tracking to consider, continuous and intermittent. Each method has its own problems.

Continuous tracking is possible, but as a general rule, most systems considered continuous are actually sampled systems operated at high acquisition rates. While the systems are not truly continuously tracking, the data rates are so high that the target moves very little from sample to sample. Very simple algorithms can correlate the target from one sample to another and the effect is basically that of continuous tracking. While continuous track systems can maintain lock on a given target, they do so at the expense of both data rate and area coverage. For an object which can move a great distance, it is often necessary to have a network of closely spaced sensors to continuously track the target.

The other mode of operation is intermittent track. Here a given sensor detects and identifies a target and reports the event to some central control or processing facility. Some time or some distance later, another sensor detects and identifies the target and similarly reports the event. The problem now is for the processing facility to correlate the two events. This becomes extremely difficult when the target cannot be uniquely identified as one specific item out of a class of items. Even with high resolution imagery, it is very difficult for automated systems to correlate two such events with high confidence. If the target is to be tracked over a large geographic area, the finite probabilities of detection, classification and identification at each sensor location make the confidence in any correlation effort rather small. Only when a target has an extremely unique signature (very high signal to noise ratio) can it reliably be tracked with an intermittent monitoring sensor network.

2.3 Why Use Tags

Tags have two basic purposes highly dependent upon the type of tag used. One use is to mark a mobile target which cannot be continuously tracked. Rather, at some point in the future, an active sensor system will sweep across a broad geographic area and the tag will generate some form of a unique reply making the target stand out. This type of operation requires a very special tag and sensing system. This is the classic "find a needle in an entire countryside of haystacks" mission.

The other basic use of tags is to mark a target giving it such a unique signature that it achieves a very high signal to noise ratio. Ideally, the tag would operate with a phenomenology and in a sensor band where noise is uncommon thereby further enhancing the effective signal to noise ratio. These tags would be applied to a target after it was properly identified by other means. Once tagged, the target achieves a highly unique signature which is easily identified exactly. This greatly improves future detection probability and all but eliminates the problem of compounding fractional probabilities during intermittent tracking.

2.4 Types of Tags

Tags come in an almost infinite variety of sizes, shapes and colors. They can be active or passive and operate over an enormous range of physical phenomenologies. They can also operate in quite a variety of ways allowing a designer to customize a particular tag to a specific mission. To briefly examine a large part of the design space, we discuss some of the phenomenologies and then look at modes of operation for electromagnetic tags.

Given a sufficient amount of time, it is quite possible that almost anything can be made into a tag. Rather than explore a multitude of specific tags, here we instead discuss some of the basic approaches and sensing phenomena.

For a tagging system to work, there must be something to sense. One obvious choice is some part of the electromagnetic spectrum. At the low end we have radio waves. In the middle there are various wavelengths of light, some visible, some not. At the high end we have X-rays and gamma rays. A tag can be made to operate virtually anywhere across this spectrum. A significant advantage of working within the EM spectrum is the very high propagation velocity for the signals involved, the speed of light. Sound can also be used as the active phenomena for a tag. In such cases, one senses the pressure wave propagating through some matter. This could range from a seismic signal propagating through the ground to an ultrasonic acoustic wave propagating through the air. The final choice would be some type of chemical or radioactive particle tag. In such cases, to sense the tagged object, it is necessary for particles, molecules or atomic fragments, to move from the target to the sensor. Such mass transport tagging approaches can be quite effective at short range but the movement of particles is highly dependent upon local atmospheric conditions.

After one has selected the phenomenology for a tag, it is necessary to consider the concept of operations and how the tag will operate. The specifics depend on the requirements of the mission. Tags can actively emit a signal, they can respond to an active query either actively or passively, or they can be completely passive giving no reaction at all.

A radio frequency (RF) tag for example might continuously or intermittently broadcast

a signal like a beacon. The advantage of such a tag is that it is easily located. The disadvantages include power consumption, possibly size and definitely covertness. Such tags continuously give themselves away.

An RF tag might also be designed to respond to a query from some type of tag interrogation system. An active responding system would include a small power supply. The device would wait and listen for a query signal. Once detected, the tag would respond with a signal of its own. However, it is also possible to build a passive or unpowered tag which responds to a query pulse. Such tags might extract power from the probe pulse and then respond, or be reactive in some way, changing the reflection of the probe pulse.

A final option is for a completely passive tag. These devices are inert with no active components. The probe pulse is in some way altered by the simple physical structure of the tag. An example would be some type of diffraction grating giving the tag a unique RF reflection characteristic not generally found on untagged targets.

Within this study, only optical tags were considered operating anywhere within the range of wavelengths from the UV through SWIR. While it is possible to build fully active optical tags and active responding optical tags, those considered here are either passive responders (fluorescence type) or completely passive approaches.

2.5 An Application

While there are an infinite variety of uses for optical tags, the research described in this report was guided by two specific potential applications. One is that of optically tagging vehicles, the other optically tagging large manufactured objects which might be moved by vehicle from a production facility to some final use location.

3 Technologies for Optical Tags

In this section we take a rather broad look at both commercial and emerging technologies which might be useful for formulating optical tags. The goal was to find suitable tagging approaches which work at visible wavelengths and then extend into some of the near visible portions of the spectrum such as the UV, near infrared and even SWIR ($\lambda < 2\mu\text{m}$) but most of the approaches found are good only for wavelengths less than $\lambda < 1\mu\text{m}$.

One interesting approach is the use of rare earth and unusual organic compounds dissolved into a binder or carrier. The narrow absorption lines of these compounds make it possible to formulate tags with unique reflection properties when viewed with a hyperspectral sensor. In addition to the well-known rare earth compounds, benzoquinolines and oligo(acetylenes) were identified as groups of organic compounds with multiple, unusually sharp, high contrast, absorption bands in the near-UV.

Another area of high interest lies in the UV as tags designed to operate at these wavelengths cannot be detected by observers without special equipment. A very crude example of a tag is for a doc worker to coat his hand with commercial sun-block and then leave his hand print on a crate. The UV absorbers in the sun-block make the hand print appear dark when imaged at UV wavelengths. However, to anyone else, the hand print is all but undetectable and easily dismissed as nothing more than a hand print. Other approaches for UV wavelengths include high contrast tags, e.g., tags that could be covert or at least low contrast in the IR, visible, or UVA and UVB, but which might be detected using deep UV sources and detectors. In addition to the benzoquinolines and oligo(acetylenes) as potential near-UV tags, triazolones and triazoles were identified as potential taggants for the $\lambda=200\text{-}250\text{nm}$ range because of their unusually narrow bands in the deep UV.

We also explore other commercial technologies useful for automated tagging and tracking. The technology review in this case is focused on commercial security technologies that might be applied to tracking with an emphasis on optical methods.

Retroreflection is perhaps the most commonly applied commercial optical security technique. However, the optimum design of such tags requires a multilayer structure with a reflective base. Corner cube reflectors and holographic reflectors would appear to be reasonable solutions, but suitable commercial sources were not found.

3.1 Focus on Commercial Technologies

Optical tagging technologies have become increasingly important as the capability for generating counterfeit products, documents, and currency has developed with the growth of computer power and the rapid growth of inexpensive scanning and printing technologies. Combinations of methods, e.g., magnetic inks, IR inks, UV fluorescent compounds, optical variable devices, etc., are all in common use. U.S. currency uses such technologies to defeat simple photocopying. However, many of the same technologies can be applied to tagging.

Optical tags may be passive, e.g., simple absorption, reactive or active, i.e., responsive to irradiation with thermal IR, near IR, visible, or UV light by mechanisms such as phase change (thermochromic materials), fluorescence, or photochromism. Examples include printed thermochromic labels used to verify that checks are originals, store receipts

that contain blue fluorescent inks to guard against counterfeiting, and some currencies that include photochromic compounds not unlike those used in plastic photochromic eyeglasses.

Remote sensing technology has also advanced rapidly with the development of increasingly sophisticated and sensitive CCD and CMOS detectors. In particular, hyperspectral sensors - sensors that record dense spectral data at each point in the field of view - offer new opportunities for remote sensing of optical tags.

Aspects of various tagging technologies are discussed below from the perspective of remote sensing. The focus is primarily on materials. Some materials are readily available; others would have to be prepared and tested for practical use as tags. In every case, the tag must be matched with a sensor - either electronic or human - to be optimally effective.

3.2 Rare Earth Oxides for Hyperspectral Tags

Many rare earth elements and their compounds, including oxides, have unique narrow band absorption and emission properties. Narrow band absorbing and fluorescent dyes are known, but with FWHM absorption bands almost universally greater than 10nm, none approach the fractional nanometer bandwidth characteristic of many bands present in rare earths. On the other hand, dyes have oscillator strengths approaching 1.0, orders of magnitude greater than the very weak bands present in the rare earths. The oscillator strengths are also reflected in the lifetime of the excited states, e.g., ~ 10 ns for dyes and ~ 1 ms for many rare earths. The fundamental reason for the difference is that transitions in the rare earths are generally spin forbidden between states involving only the f-shell electrons that are shielded from the local environment. Dye transitions are generally inhomogeneously broadened by the local environment and are symmetry-allowed. Even formally forbidden symmetric transitions in dyes often have high oscillator strengths and short lifetimes due to local deviation from perfect symmetry. Below we briefly examine some of the available materials and their characteristics. For a detailed discussion of spectral tagging, interested readers should consult other sources [1].

Data on the spectral characteristics of rare earth oxides were found in documents relating to optical filter glass, luminescent optical glass and standard reference materials for spectrometers. Optical filter glass containing didymium as well as other elements have long been used by glassblowers to reduce the blindingly bright sodium flare of hot glass. Other glasses have often been used to increase contrast and color gamut in displays, including CRTs. Hyperspectral, narrow band absorption is not necessarily required in either of these applications.

Luminescent optical glass is related to phosphors. Europium+3 based phosphors are commonly used in lighting, but especially in CRTs (for red). Recently, however, there has been increased interest in rare earths in their "reduced" +2 states. The spectroscopy the elements in the reduced states is, as expected, much different than that of the oxidized state. The difficulty has, until recently, been that the rare earths oxidize during glass or phosphor processing. However, new non-oxidizing glass formulations have led to the development of bright, blue emitting Eu+2 based glasses, e.g., Lumilass from Sumita Optical.

Stabilization of such dicationic states in organic chelates of the rare earths is probably difficult in air. Organic chelates of the rare earths were studied as a possible means of

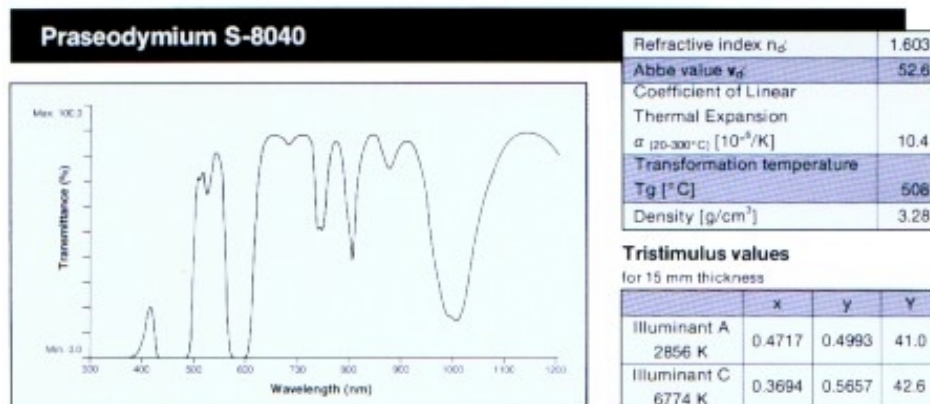


Figure 1: Low resolution transmission curve for Schott rare earth oxide doped glass Praseodymium S-8040 [2]

fabricating inexpensive or disposable laser rods (this application apparently did not meet expectations) and much of this science is now 30 or more years old. Organic chelates or the rare earths offer an excellent potential method of molecular dispersal of rare earths in plastic (polymeric) tags because such materials can be designed to efficiently absorb light, and, for certain elements, luminesce in the green (terbium) or red (europium) after energy transfer from the ligands to the central metal.

Another option for a rare-earth based formulation of an optical tag (based on the availability of materials) is the dispersion of rare earth oxides in a polymer matrix. The oxides are available commercially as $5\mu m$ powders. Such powders can probably be dispersed into a polymeric carrier efficiently with ultrasound; however, the dispersion may settle with time. A high viscosity carrier is less likely to allow settling. Although Lumilass is available only as a plate, it can probably be ground into a fine powder.

Representative spectra for individual and combined rare earth oxide materials are shown in the Figures 1 to 11. The Schott website [2] provides low resolution spectral curves of their rare earth oxide glasses that give the reader a quick overview of the gross spectral properties of these materials.

A wavelength standard for infrared spectrometers is provided in the Standard Reference Material (SRM) 2035 from the National Institute of Standards and Technology (NIST) [3]. This material consists of a mixture of rare earth oxides, each of which has several sharp absorption bands in the infrared. A mixture of commercially available rare earth chelates in a suitable solvent or binder would probably provide a similar spectrum in the same $\lambda \sim 900$ -4000nm range, and probably without the scattering that would result from an insoluble-oxide filled binder. A spectrum of SRM 2035 is shown in Figure 12.

A high-resolution visible - through deep UV spectrum of Ho+3 in perchloric acid solution is shown in Figure 13 with the peaks identified in Table 1. Far more detail is apparent in this spectrum than in that for the Schott glass as seen in Figure 8.

Tremendous efforts have been put into developing brighter, more energy efficient phosphors for applications from displays, e.g., plasma display panels, to white LEDs. Two leaders

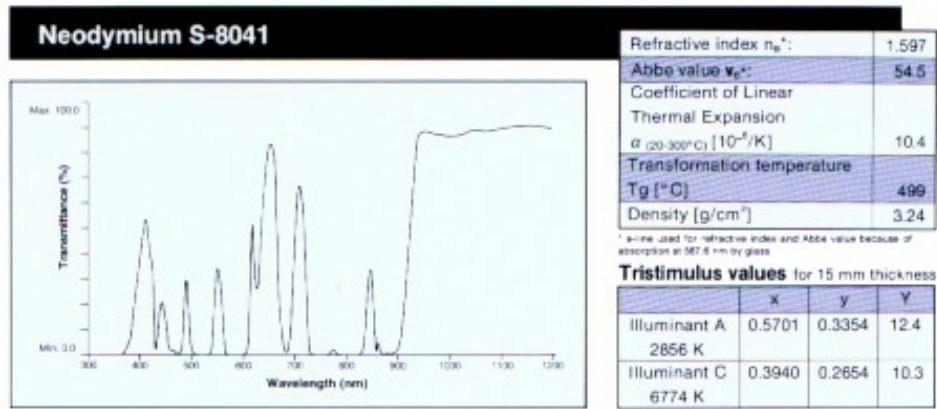


Figure 2: Low resolution transmission curve for Schott rare earth oxide doped glass Neodymium S-8041 [2]

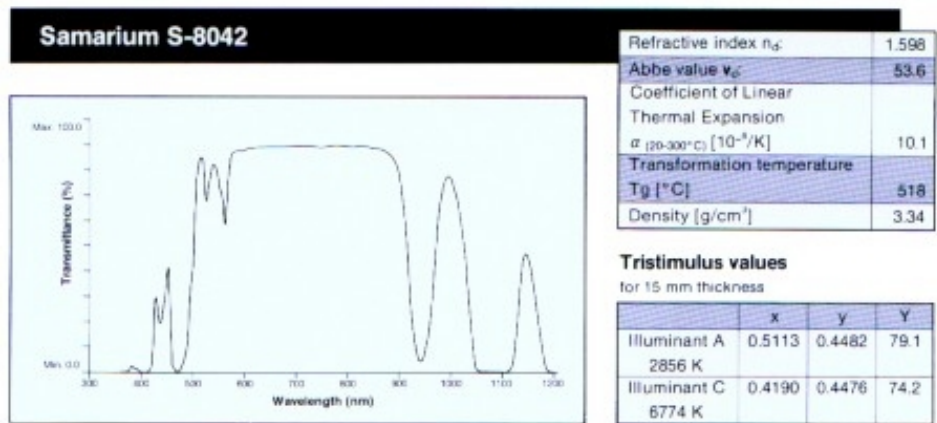


Figure 3: Low resolution transmission curve for Schott rare earth oxide doped glass Samarium S-8042 [2]

Short UV Region	Long UV Region	Visible Region
241.0nm	333.5nm	416.1nm
249.9nm	345.6nm	451.1nm
278.2nm	361.4nm	467.8nm
287.1nm	385.4nm	485.2nm
		536.6nm
		640.6nm

Table 1: Spectral peaks for Holmium corresponding to those shown in Figure 13.

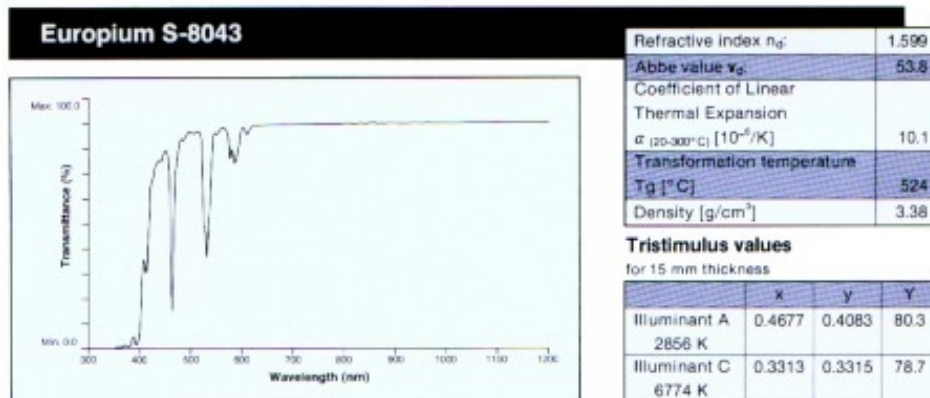


Figure 4: Low resolution transmission curve for Schott rare earth oxide doped glass Europium S-8043 [2]

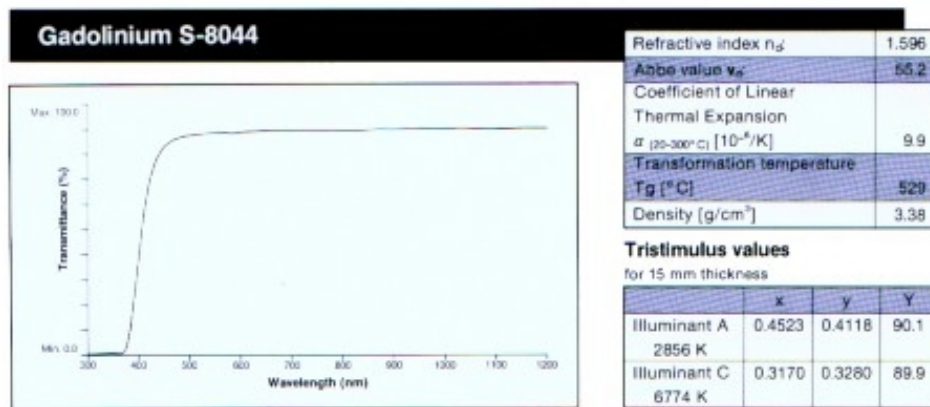


Figure 5: Low resolution transmission curve for Schott rare earth oxide doped glass Gadolinium S-8044 [2]

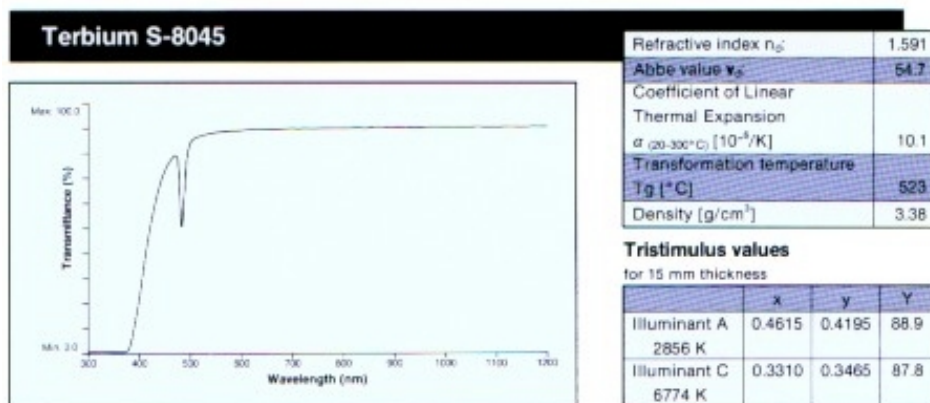


Figure 6: Low resolution transmission curve for Schott rare earth oxide doped glass Terbium S-8045 [2]

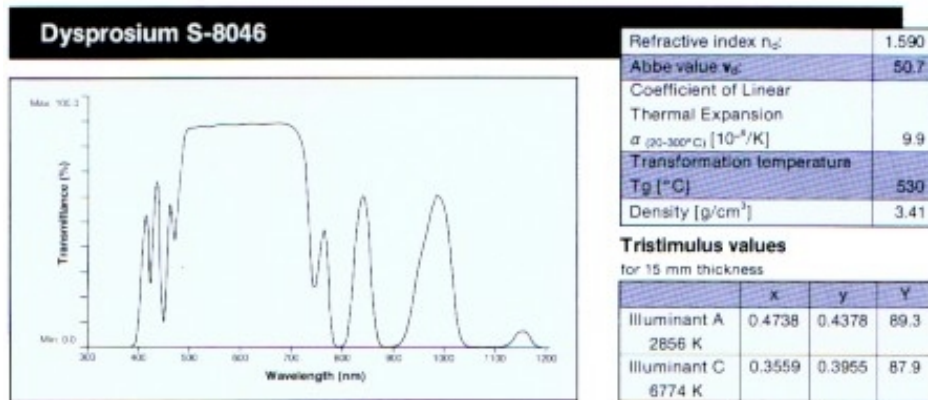


Figure 7: Low resolution transmission curve for Schott rare earth oxide doped glass Dysprosium S-8046 [2]

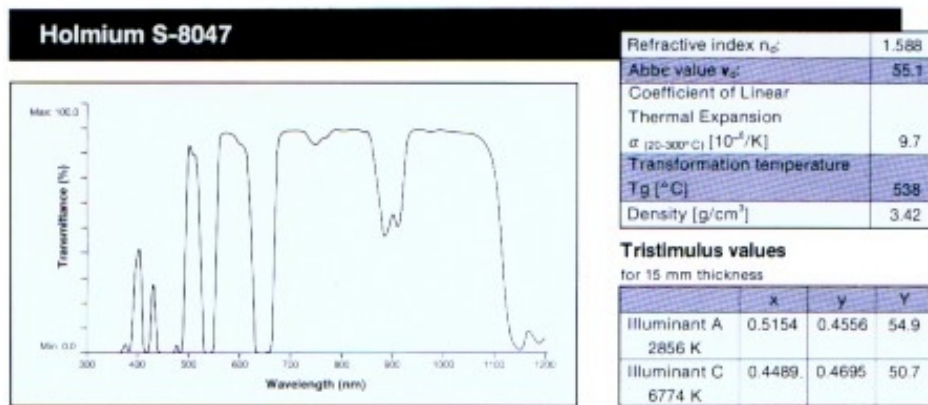


Figure 8: Low resolution transmission curve for Schott rare earth oxide doped glass Holmium S-8047 [2]

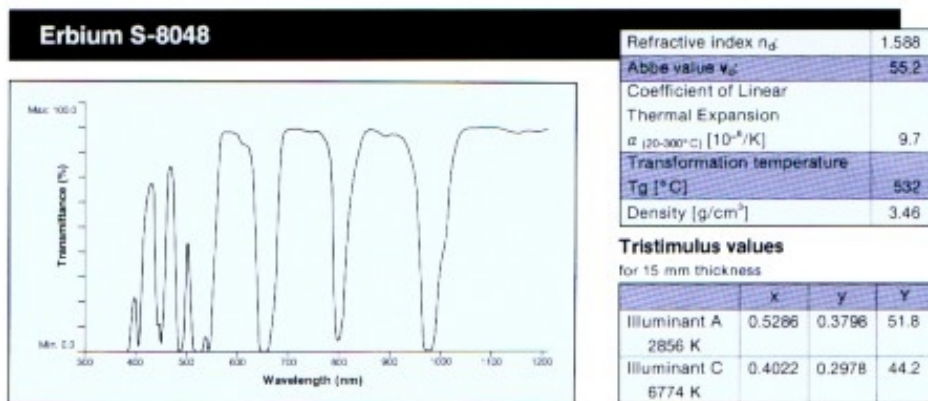


Figure 9: Low resolution transmission curve for Schott rare earth oxide doped glass Erbium S-8048 [2]

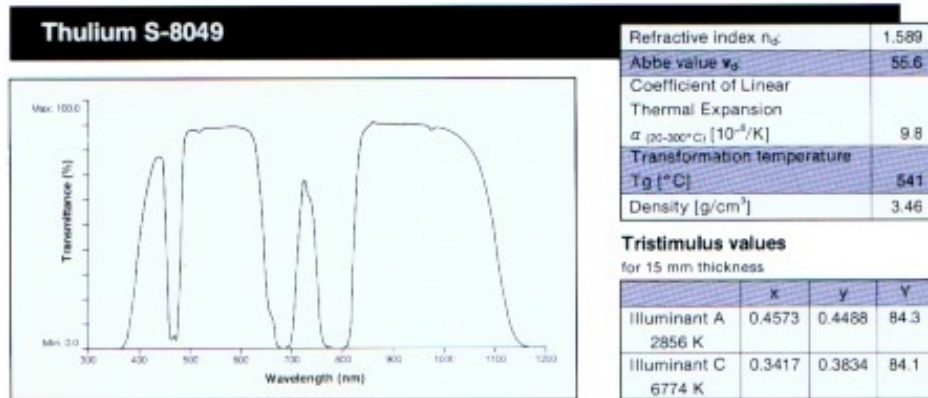


Figure 10: Low resolution transmission curve for Schott rare earth oxide doped glass Thulium S-8049 [2]

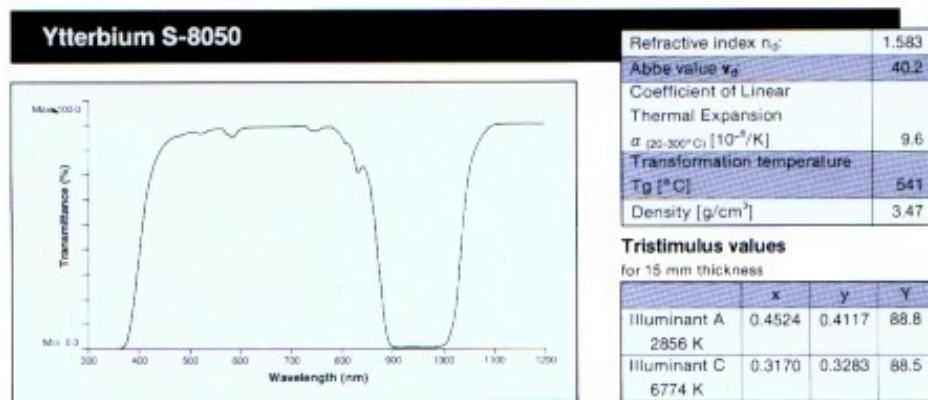


Figure 11: Low resolution transmission curve for Schott rare earth oxide doped glass Ytterbium S-8050 [2]

UV Region	Visible Region	Near IR Region
289.0nm	444.1nm	731.8nm
329.0nm	468.7nm	740.1nm
354.0nm	481.8nm	794.1nm
	512.0nm	801.2nm
	521.3nm	865.0nm
	574.9nm	

Table 2: Spectral peaks for Didymium corresponding to those shown in Figure 14.

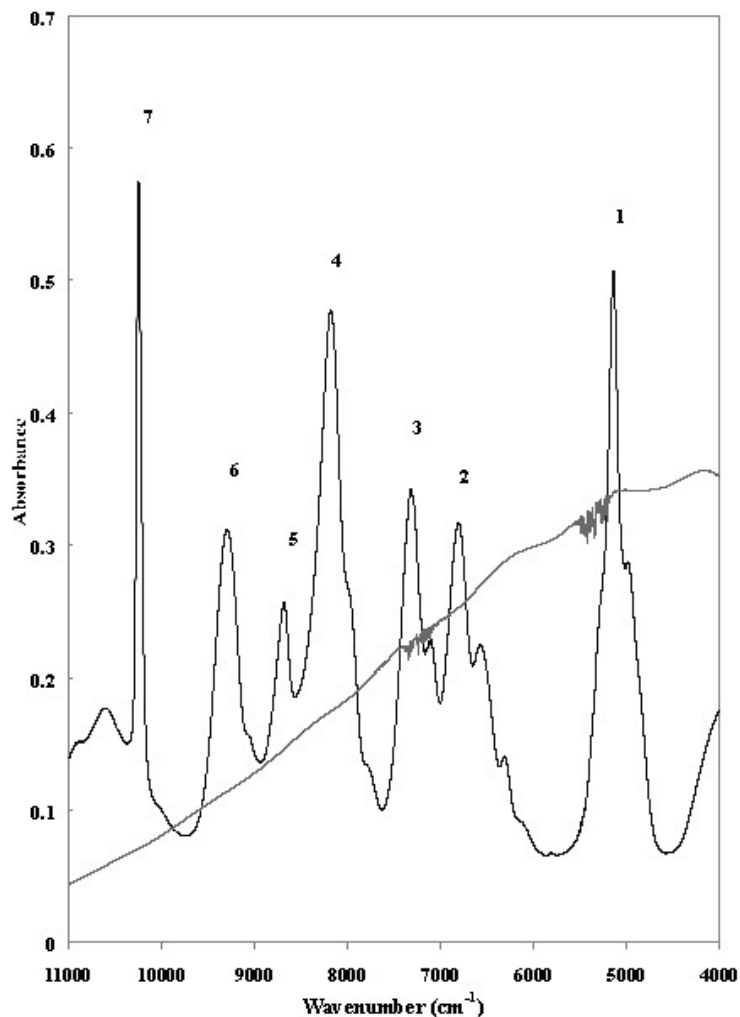


Figure 12: An example of complex spectral patterns in the near-IR that are available from mixtures of rare earth oxides. Spectrum of a glass optical filter designed containing several rare earth oxides to provide well defined absorbance features from $10,000\text{cm}^{-1}$ to $5,000\text{cm}^{-1}$. The filter glass contains 3.00 mole % Ho_2O_3 , 1.30 mole % Sm_2O_3 , 0.68 mole % Yb_2O_3 , and 0.47 mole % Nd_2O_3 . These concentrations were chosen to yield peak absorbances between 0.2 and 0.6 with 1.5mm thick filters [4,5]. Precise reference band positions are published in the Certificate for SRM 2035 [6].

Short UV Region	Long UV Region	Visible Region
235.2nm	305.3nm	401.5nm
266.7nm	317.6nm	415.2nm
279.1nm	331.7nm	441.2nm
280.2nm	344.6nm	463.5nm
		478.5nm

Table 3: Spectral peaks for Samarium corresponding to those shown in Figure 15.

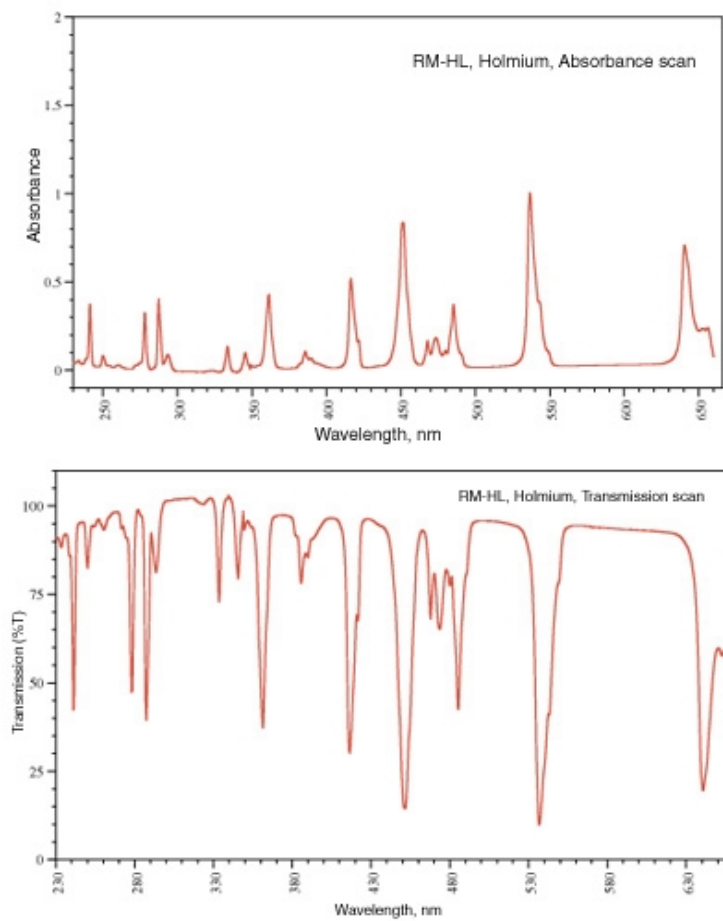


Figure 13: Transmission and absorption spectrum for Holmium which has one of the most complex spectra of any rare earth material. These data are for Holmium oxide, 4%, in perchloric acid solution, 10% with a 1cm path length [7]. The data shown here reveal the details not visible in the Schott spectra (Figure 8). Details of the spectral peaks are given in Table 1.

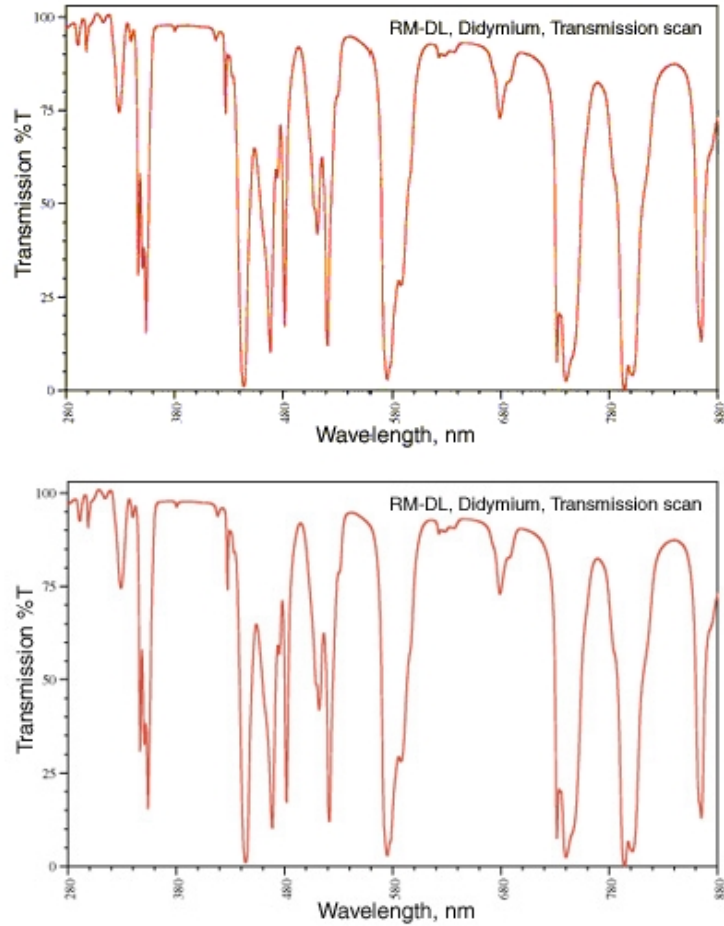


Figure 14: Didymium’s absorption spectrum is also complex. Note the strong absorption near $\lambda=580-600\text{nm}$ that removes the sodium flare in glassblowers’ glasses [7]. Spectroscopic details of liquid samples are more pronounced in those for Schott glasses. Details of the spectral peaks are given in Table 2.

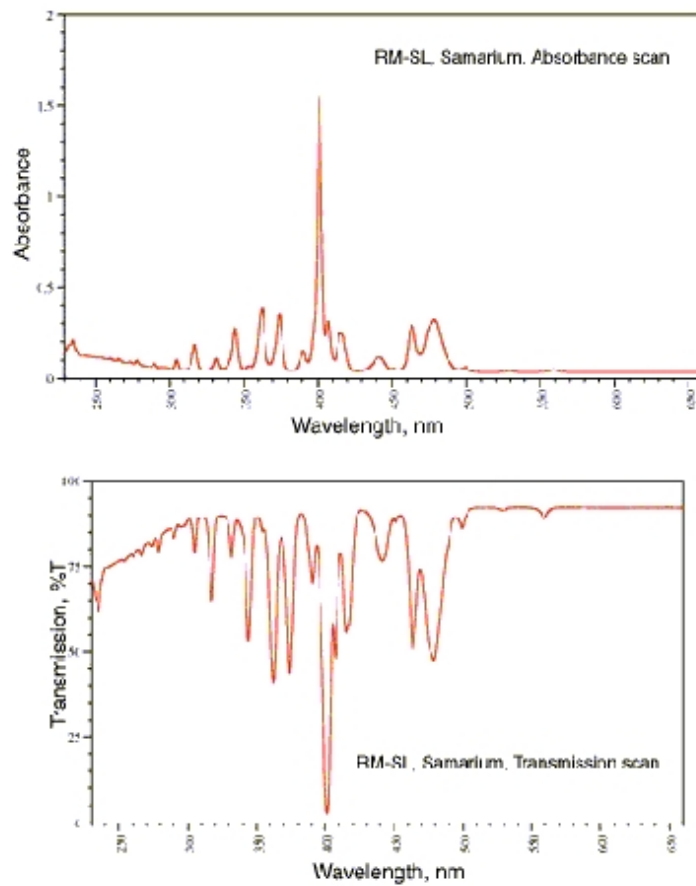


Figure 15: The Samarium absorption spectrum is characterized by one very strong peak with many weaker bands [7]. A pronounced spectral line occurs at about $\lambda=400\text{nm}$ which is most obvious in the absorption spectrum. Details of the spectral peaks are given in Table 3.

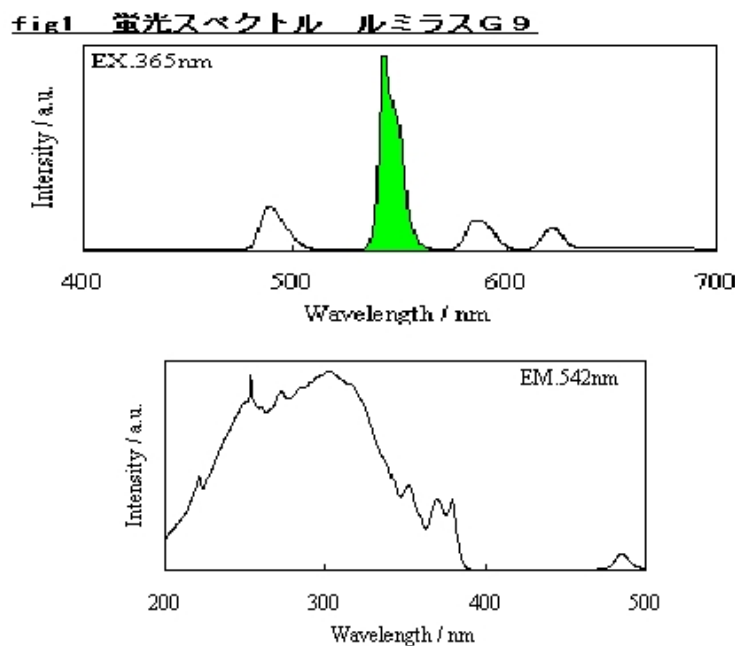


Figure 16: Luminescent Lumilass G9 emission (above) and excitation spectrum (below) [8]. Sumita claims exceptional brightness for this terbium based glass - ten times the efficiency of what they claim for the blue and red glasses.

in this area are Nichia and Osram-Sylvania. Other companies have also developed new technologies such as coated phosphors that show higher quantum yields for fluorescence than uncoated phosphor particles.

Other examples of recent advances in luminescent materials are the glasses that have been developed by Sumita Optical Glass. These monolithic glasses appear to be unique products with bright red, green and blue emission. Emission and action spectra of these glasses are shown in Figures 16, 17 and 18, all taken from Sumita’s web site [8]. Sumita claims that “Irradiating $\lambda=365\text{nm}$ ray of $120\text{mW}/\text{cm}^2$ to a spot of 20mm in diameter, LUMILASS-G9 can emit the brightness of $10,000\text{ lux}$, and LUMILASS-R7 and LUMILASS-B can emit $1,000\text{ lux}$.”

3.3 UV Fluorescent or Hyperspectral Tags Based on Organic Compounds

UV fluorescent tags, e.g., UV absorbing, visible-emitting, dyed or pigmented inks, are common commercial items and UV fluorescent inks are widely available in many colors. Stability of the dyes toward UV irradiation varies widely with many applications not requiring more than incidental UV stability (receipts, hand-stamps, chemiluminescent glow sticks, and other disposable applications). Higher stability is required of scintillating compositions and in applications where solar exposure is required. Major suppliers of such dyes include BASF and Clariant, and there are innumerable sources of formulated fluorescent inks.

fig 3 蛍光スペクトル ルミラスR7

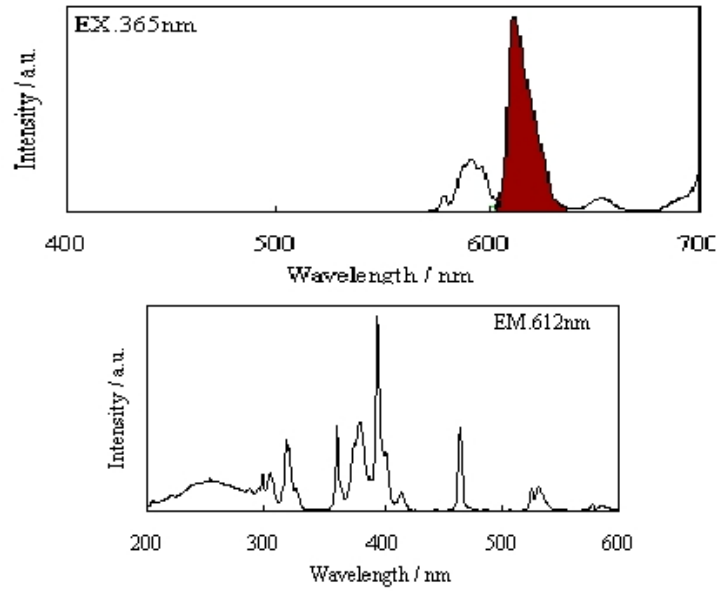


Figure 17: Emission and excitation spectra for the europium based glass R7 [8].

fig 5 蛍光スペクトル ルミラスB

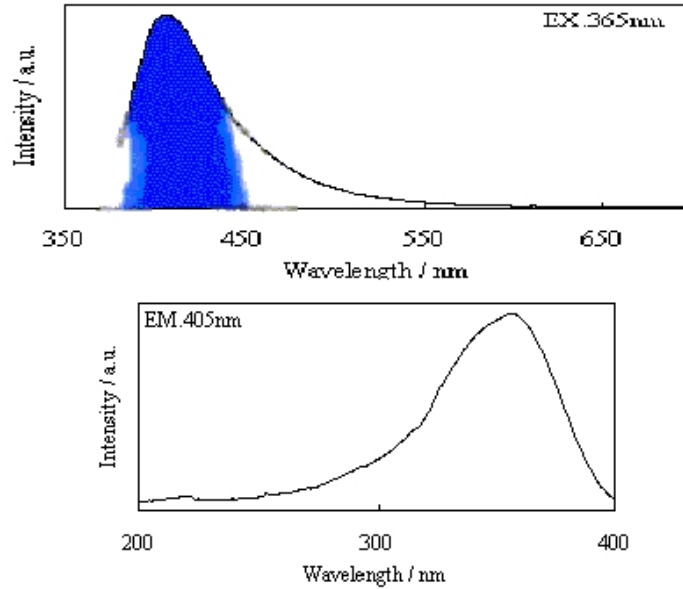


Figure 18: Emission and excitation spectra of Lumilass B [8]. The emitting ion is probably europium +2.

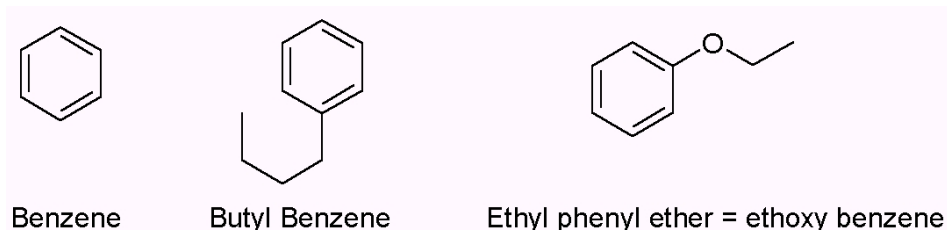


Figure 19: Benzene, alkyl benzenes and alkoxybenzenes.

A covert approach UV tagging might apply UV absorbing compounds with distinctive absorption and/or fluorescence properties. The key in such an approach would be a unique optical signature that is not present in nature and not easily confused with signals from natural sources. Arguably the best approach to such unique tags is via compounds that have multiple unique absorption or fluorescent features in their UV spectra.

The advantage that organic compounds (dyes) have over rare earths is in their very much higher absorption cross-section or molar absorptivity. The disadvantage of the organic dyes was discussed in the previous section: almost all dyes have far broader absorption bands than exhibited by rare earth compounds. However, several classes of organic compounds show unusually narrow bands that are potentially very useful for the preparation of unique, hyperspectral UV tags. Examples of each of these classes of compounds are shown below.

Several excellent reference series are available with graphed spectra for inspection. These compendia are generally organized by molecular weight or molecular complexity. Therefore a page-by-page review of thousands of spectra was performed in order to select the most likely candidates for both near and deep UV tags. Compounds with narrow absorption features in the UV are organized into sections 3.3.1 to 3.3.6 below.

3.3.1 Isolated Carbocyclic Ring Compounds

Benzene, alkyl benzenes, and alkoxybenzenes as shown in Figure 19 all exhibit relatively unique absorption spectra with multiple, relatively sharp absorption bands as seen in Figure 20. These bands appear to be derived primarily from vibrational excited states. These compounds as a class are also weakly fluorescent in the UV. Unfortunately, such compounds are present in gasoline and in many natural (plant) products and therefore may be less unique than other materials.

3.3.2 Condensed Carbocyclic Ring Compounds

The spectra of naphthalene and its derivatives possess relatively broad absorption features. Surprisingly, the next larger condensed ring system, anthracenes, give spectra with much more distinctive absorption bands. The compounds are generally fluorescent in the UV to blue spectral ranges; however, the emission can be shifted into the green by proper substitution. A wide variety of anthracenes are commercially available and inexpensive. Anthracene derivatives have been (and may still be) used in blue and green chemiluminescent "glow sticks".

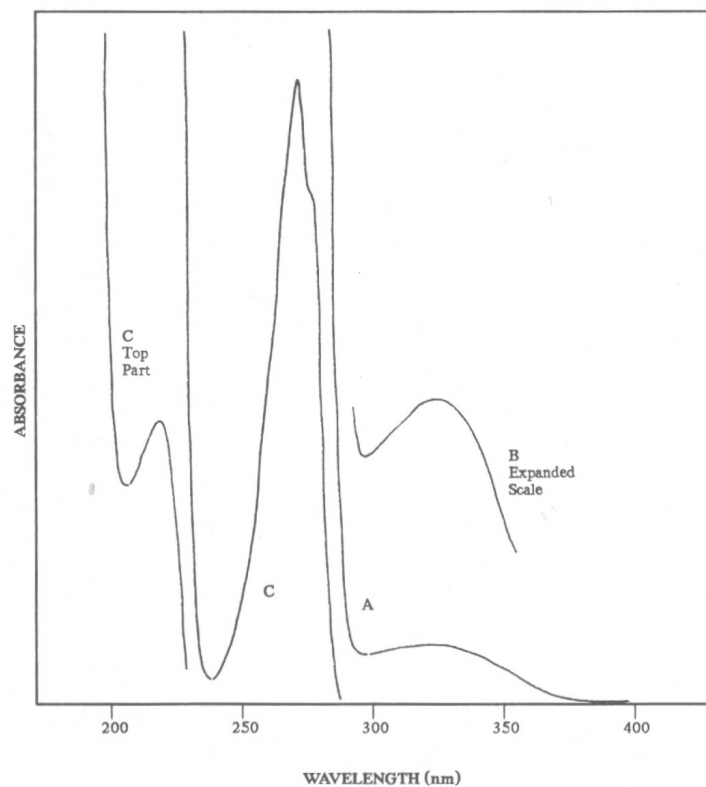


Figure 20: The ultraviolet spectrum of ethyl phenyl ether in ethanol at a concentration of 5×10^{-3} moles per liter consists of a single strong peak near $\lambda=270\text{nm}$ with weaker features in the $\lambda=300\text{-}350\text{nm}$ range. Line "C" is a 0.01cm path length, line "B" is 0.1cm path length and line "A" is for a 1.0cm path length [9]. The spectra of other alkoxy-substituted benzenes are similar.



Figure 21: Structures of condensed carbocyclic ring compounds.

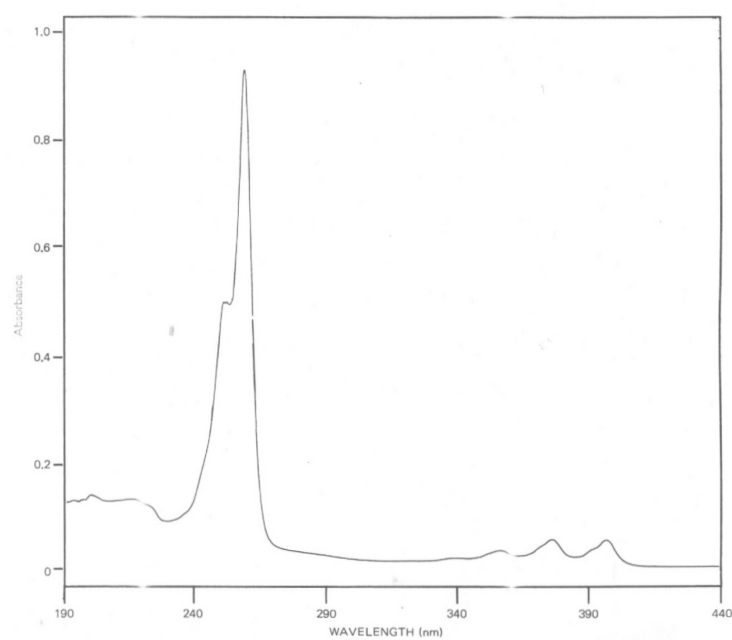


Figure 22: The ultraviolet spectrum of 9,10-dimethylantracene in absolute ethanol at a concentration of 1.152×10^{-5} moles per liter consists of a single strong peak near $\lambda=260\text{nm}$ with weaker features in the $\lambda=350\text{-}400\text{nm}$ range [9]. The spectra of other alkyl-substituted anthracenes are similar.



Figure 23: Structures of condensed heterocyclic ring compounds.

Anthracenes are probably good choices for UV tags in cases where weak blue emission is acceptable or desirable. Representative chemical structures are seen in Figure 21 with spectra seen in Figure 22.

3.3.3 Condensed Heterocyclic Ring Compounds

Among the most distinctive and unusual spectra are those of "aza-phenanthrenes" or benzoquinolines. All three of these compounds exhibit a pair of extremely narrow and distinct absorption bands at about $\lambda=330\text{nm}$ and $\lambda=345\text{nm}$. The bandwidth of these absorption features, measured as their full-width-half-maximum values in absorbance, is less than 4nm. Such absorption features are virtually unknown outside of metal-centered transitions that are observed for some rare earth and transition metal complexes.

The distribution of these compounds in the environment is unclear. However, the USGS has observed phenanthridine in μg per kg concentrations in the environment. Representative chemical structures are seen in Figure 23 with spectra seen in Figure 24.

3.3.4 Compounds with isolated double bonds between heteroatoms

The deep UV spectra of compounds with isolated double bonds between first and second row elements frequently show relatively narrow peaks that are well separated from other absorption features. Some examples of such compounds are shown in Figure 25 with representative spectra shown in Figures 26 and 27.

Another compound that shows a similar minimum in absorption in the deep UV is tris(*o*-tolyl)-phosphine oxide. In dilute ethanol solution, the compound has neighboring maxima at $\lambda=272\text{nm}$ and $\lambda=279\text{nm}$ ($e = 3,000$ and $2,950$) with a minimum absorbance at about $\lambda=248\text{nm}$ with $e \sim 150$ L/M-cm. Therefore the contrast ratio in molar absorptivity is about 20:1. In other words, for an solution of this molecule with an optical density of 2 (99% absorbing) at $\lambda \sim 272\text{nm}$, the solution would be 97% transparent at $\lambda \sim 248\text{nm}$.

The data for these two compounds share a common feature of a double bond between a first and a second row element. Other phosphine oxides and thioamides may show similar high contrast spectra in the deep UV.

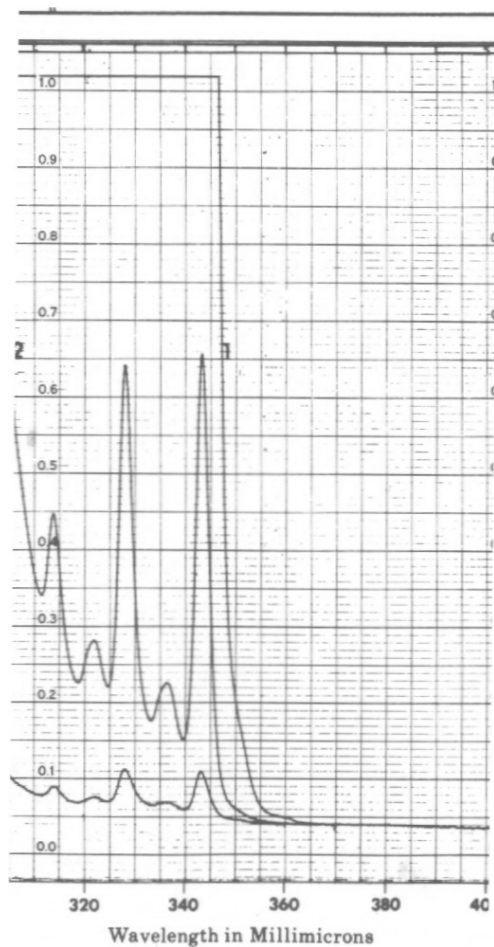


Figure 24: The ultraviolet spectrum of phenanthridine in the $\lambda=300-400\text{nm}$ region shows two especially narrow peaks at about $\lambda=328\text{nm}$ and $\lambda=343\text{nm}$. The full width at half maximum of these peaks is about 4nm - among the sharpest peaks of any organic molecule. The contrast ration in absorbance is not as high as other compounds discussed in this report, however. Other benzoquinolines show similar spectra. The spectra were taken in cyclohexene at the following concentrations: (1) $0.4886\text{ grams/liter}$, (2) $.04886\text{ grams/liter}$, (3) lowest, $0.00489\text{ grams/liter}$ in a 1cm path length [9].

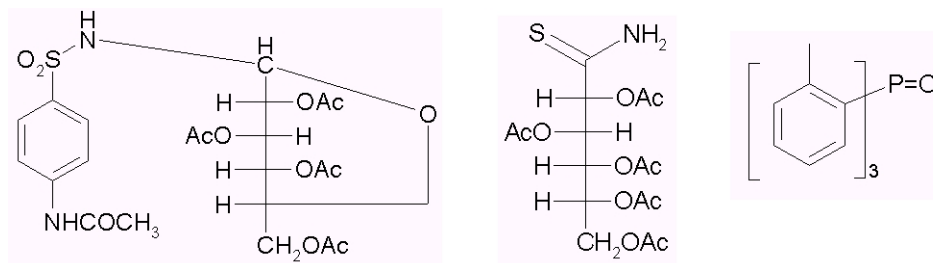


Figure 25: From left to right: N-(4-acetamidobenzenesulfonyl)-D-glucosylamine-2,3,4,6-tetraacetate), pentaacetyl-D-thiogluconoamide, and tri(o-tolyl)phosphine oxide.

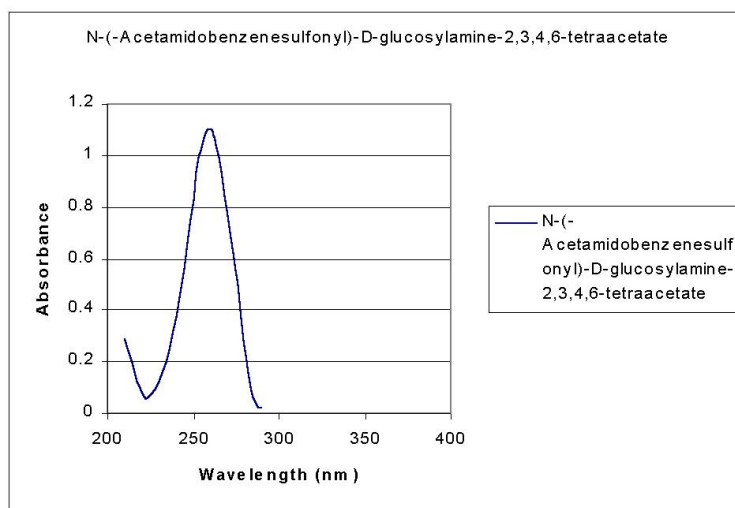


Figure 26: Example of a compound with a dip in absorbance in the UV that could be used as a high contrast tag by comparing reflectance at $\lambda \sim 230\text{nm}$ and $\lambda \sim 275\text{nm}$. The full width at half maximum is about 32nm. The contrast is about 14:1. Relatively few compounds show this degree of contrast in the deep UV. The concentration of the solute was 5×10^{-5} moles per liter (molecular weight 544.5) in ethanol with a 1cm path length [9].

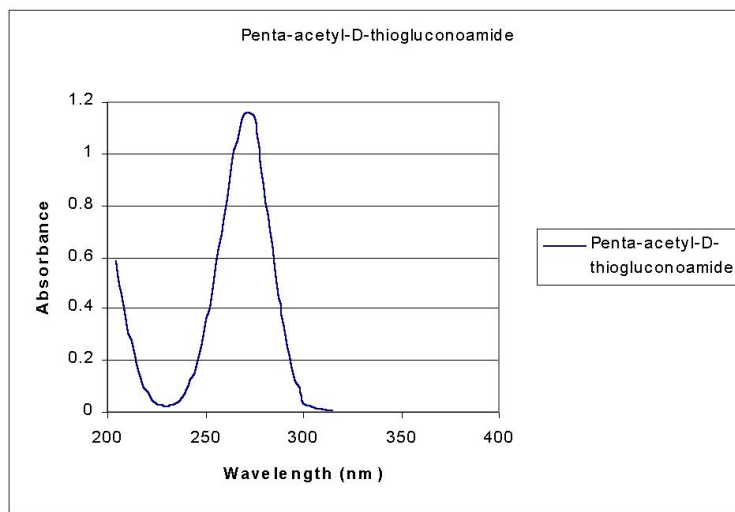


Figure 27: Second example of a compound with a dip in absorbance in the UV that could be used as a high contrast tag by comparing reflectance at $\lambda \sim 230\text{nm}$ and $\lambda \sim 272\text{nm}$. The full width at half maximum is about 30nm. The contrast is about 53:1. Very few compounds show this degree of contrast in the deep UV. The concentration of the solute was 1×10^{-4} moles per liter (molecular weight 421.5) in ethanol with a 1cm path length [9].

3.3.5 1, 2, 4-Triazol-3-ones and Related Compounds

Triazoles are 5 membered ring compounds with 2 carbons and 3 nitrogen atoms. Two examples of such compounds are shown in Figure 28. The triazoles and triazolones both have a single strong absorption near $\lambda = 225\text{nm}$ in the deep UV. Representative spectra are shown in Figure 29.

3.3.6 Oligo(acetylenes)

Oligo(acetylenes) such as the tetra-yne shown in Figure 30, exhibit narrow, nearly equally spaced, absorptions. For the molecule in the Figure 30, these absorptions appear at $26,900\text{cm}^{-1}$, $28,800\text{cm}^{-1}$, $31,000\text{cm}^{-1}$, and $33,200\text{cm}^{-1}$ (372nm , 347nm , 323nm and 301nm) and are sep-

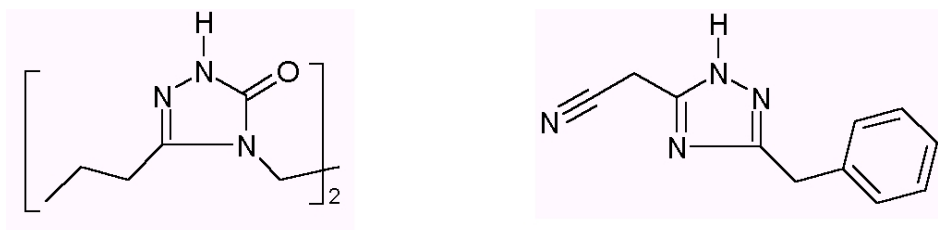


Figure 28: 4,4'-(1,2-ethanediyl)bis(2,4-dihydro-5-propyl-3H-1,2,4-triazol-3-one) and [(5-phenylmethyl)-2H-1,2,4-triazol-3-yl]ethanenitrile.

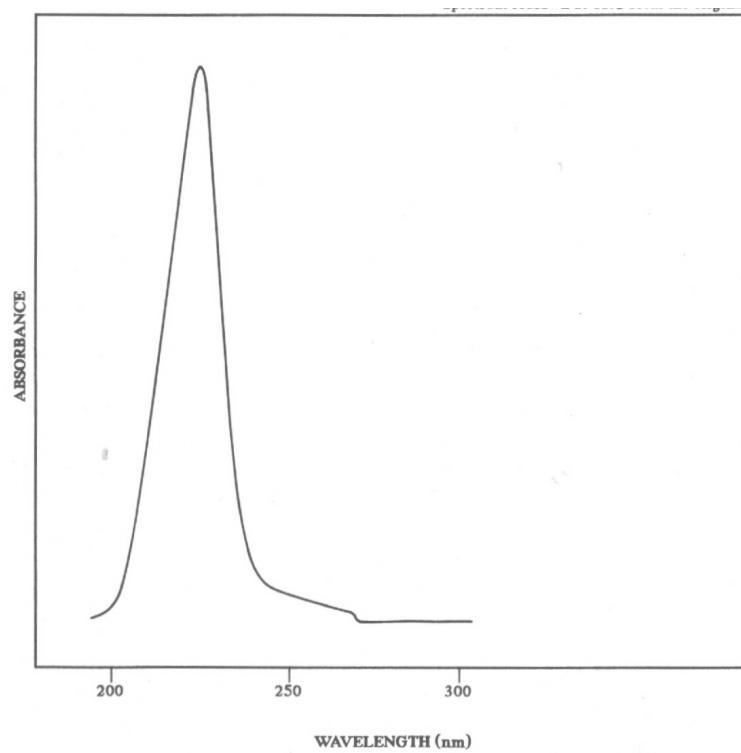


Figure 29: Ultraviolet spectrum of 4,4'-(1,2-Ethanediy)bis(2,4-dihydro-5-propyl-3H-1,2,4-triazol-3-one) in ethanol at a concentration of 1.0mg/mL. The absorbance scale is arbitrary. The peak is at about $\lambda=225\text{nm}$ with a full width at half maximum of about 20nm. The spectra of other triazolones are similar [9].



Figure 30: 2-Chlorotrideca-3-ene-5,7,9,11-tetraen-1-ol.

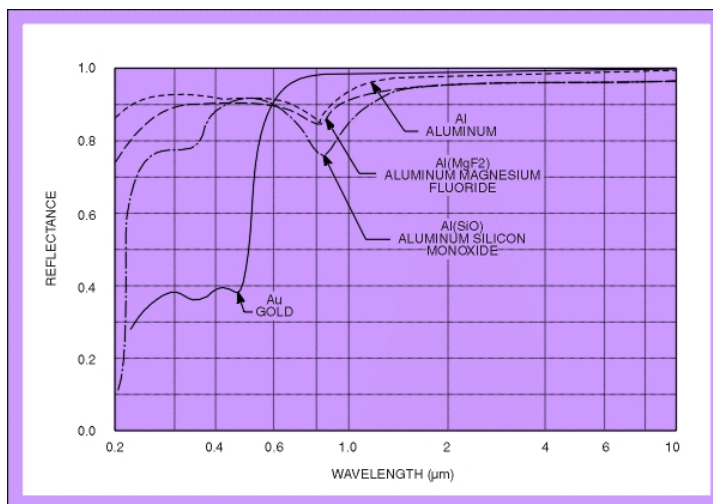


Figure 31: Reflectivity data from Oriel "Book of Photon Tools". Most Retroreflectors require a thin metal reflector. Aluminum is an inexpensive and effective deep UV reflector. [10].

parated from each other by minima with about 10% of the absorbance of the peaks. All four peaks have absorbances of about 10,000.

3.3.7 Reflectivity of the Underlying Surface

A high contrast, non-fluorescent, UV-absorbing tag should be applied to a surface with at least some UV reflectivity, otherwise it will be the equivalent of a black tag on a black background. Aluminum and rhodium have extremely high reflectivity in the deep UV and are particularly useful. The charts below from the Oriel "Book of Photon Tools" [10] are indicative of the reflectivity of metal surfaces.

Some polymeric surfaces are also likely to be highly reflective, although data in the $\lambda=200-300\text{nm}$ region was not found. Scattering surfaces of poly(ethylene), other aliphatic polyolefins, fluorocarbons such as Teflon®, probably appear bright in the deep-UV. On the other hand, polystyrene, ABS (a common copolymer of acrylonitrile, butadiene and styrene), PMMA or Plexiglas, polycarbonate or Lexan®, PVC (because of additives), and most paints, natural products and natural surfaces probably appear highly absorbing or dark between $\lambda=200$ and 250nm .

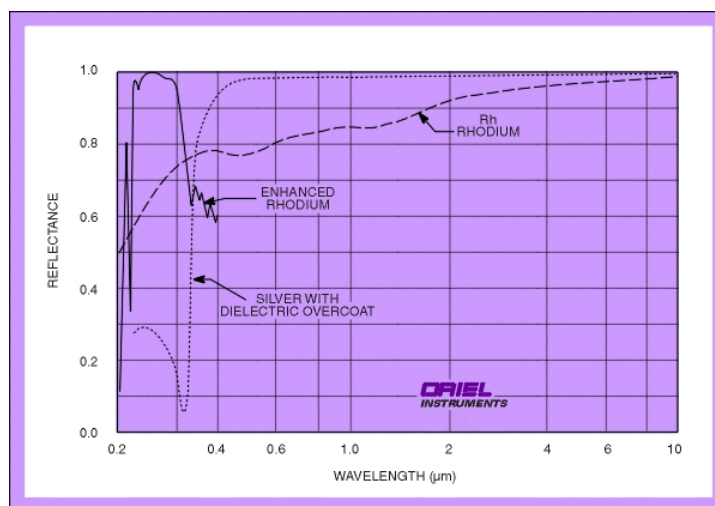


Figure 32: Reflectivity data from Oriel "Book of Photon Tools". Most Retroreflectors require a thin metal reflector. Aluminum is an inexpensive and effective deep UV reflector. [10].

3.3.8 Hosts for Deep UV Tags

A deep UV tag cannot in general be applied as a pure substance to a surface because intermolecular interactions nearly always broaden out the narrow band absorbance features that make the tag useful. Instead, the taggant molecule must be dissolved, generally at about 1% by weight or less in a carrier solvent. What is important in Table 4 is that simple aliphatic compounds such as saturated hydrocarbons (including pure mineral oils), saturated hydrocarbon alcohols, ethers, and nitriles are probably the best hosts or diluents for the UV tags. It was not possible to locate information on silicone fluids. Such fluids are often high purity, but poor solvents for most organic compounds. Other transparent binders include fluorocarbon oils such as 3M's Fluorinert®. Fluorinated resins have spectra representative of such compounds. See the spectrum of Teflon AF®, below. Cytop® resins from Asahi Chemical probably show similar spectra. More recent developments include polymers for deep-UV (for wavelengths between 157nm and 193nm) photoresists. Such polymers must be substantially transparent to UV radiation.

3.3.9 Other UV Tags

Retroreflective tags are potentially useful for search and track applications because of the strong return from such devices. Most retroreflective tags are based either on high index beads above a reflective surface or on an embossed, corner-cube-like reflective surface. Variations on this theme are glass beads trapped or embedded into fabrics.

Such retroreflective tags could be covert to the eye or night vision goggles if the tag were covered by a UV-transparent but visible/IR absorbing layer, or if the outermost component of the tag were UV transparent but visible/IR absorbing. UV transparent coatings can be difficult to design if they need to have broad visible through NIR absorbance. Dyes with strong visible absorbance but low absorbance in the UV were not identified in this study.

Solvent	λ_{CutOff}	Solvent	λ_{CutOff}
Acetone	330nm	Glyme	220nm
Acetonitrile	190nm	Heptane	200nm
n-Butyl Acetate	254nm	Hexadecane	190nm
n-Butyl Alcohol	215nm	Hexane	195nm
n-Butyl Chloride	220nm	Iso-Octane	215nm
Chlorobenzene	287nm	Isobutyl Alcohol	220nm
Chloroform	245nm	Isopropyl Alcohol	205nm
Cyclohexane	200nm	Methanol	205nm
Cyclopentane	198nm	2-Methoxyethanol	210nm
o-Dichlorobenzene	295nm	Methyl t-Butyl Ether	210nm
Dichloromethane	233nm	Methyl Ethyl Ketone	329nm
Dimethyl Acetamide	268nm	NMP	285nm
DMF	268nm	Pentane	190nm
DMSO	268nm	Propylene Carbonate	220nm
Dioxane	215nm	THF	212nm
Ethyl Acetate	256nm	Toluene	284nm
Ethyl Alcohol	210nm	Water	190nm
Ethyl Ether	215nm	o-Xylene	288nm
Ethylene Dichloride	228nm		

Table 4: Solvent Cut-off Wavelengths (Wavelengths where A=1 in 1 cm) for Pure Solvents [11].

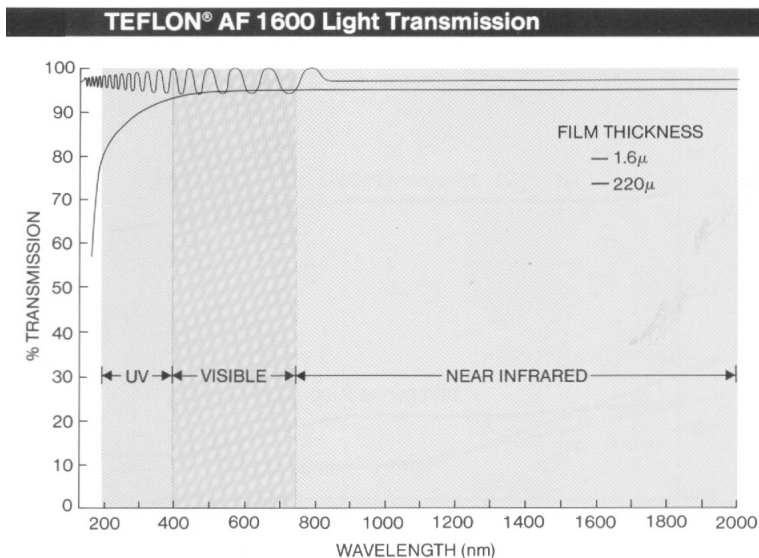


Figure 33: A deep UV optical tag may require a transparent binder. Transparency in the deep UV requires that most or all of the binder be free of double bonds. TeFLON® AF, a product of du Pont, is composed entirely of C-F, C-C, and C-O bonds and has good transparency in the deep UV. Unfortunately, it is a poor solvent for other materials and like TeFLON® PTFE, is difficult to adhere to surfaces. Polymers such as poly(vinyl alcohol) but with crosslinks to form a tough material may be more effective.

Optically Variable Pigments (OVPs) comprise a large number of multilayer dielectric particles that are manufactured by, among others, BASF (inorganic Variochrome and Paliochrome pigments) and Wacker (cholesteric liquid crystal based pigments). These pigments are popular components of security coatings because their reflected color varies with perspective. A common example of an OVP ink is the green-to-black color change on the numerals on the U.S. \$20 bill.

Inorganic multilayer dielectric pigments could be fabricated for the UV, but no commercial examples were identified. Organic multilayer dielectric pigments would be more challenging to design for the UV because of the absorbance of the UV absorbance of the cholesteric liquid crystal components. No examples of such pigments were identified.

Organic multilayer dielectric pigments take two general forms. One form is marketed by 3M and consists of alternating layers of polymers with a large difference in index of refraction. The most interesting optical effects occur in birefringent systems, "giant birefringent optics" or GBOs [12]. A kit consisting of several types of GBOs is available from 3M for \$100.

The other form of organic multilayer dielectric pigments are marketed by several companies, not all of which acknowledge the use or manufacture of such pigments because of applications in security coatings. Other applications for the cholesteric polymers include automotive paint pigments and quarter wave plates for liquid crystal displays. Cholesteric liquid crystals selectively reflect, or more precisely, diffract, one "handedness" of light and transmit the other "handedness". The pass band of the liquid crystal is determined by the difference in refractive index between the ordinary and extraordinary rays of the polymer

and the center wavelength is determined by the pitch. The pitch is, in turn, determined by the helical rotatory power and concentration of the chiral dopant.

3M markets a series of chiral films for liquid crystal displays under the Vikuiti™ name. Sample kits are available from 3M.

Helicones® are cholesteric pigments manufactured by Wacker and sold in the U.S. by Seegott. These pigments are available in a range of "colors", i.e., center wavelengths, and diameters. All of the author's attempts to alter the center wavelength by swelling the Helicones® with either a chiral dopant, or a nematic liquid crystal, or an isotropic solvent, failed to induce a color change. These results suggest that the pigments are tightly crosslinked.

There are no fundamental reasons why cholesteric polymers could not be manufactured with reflection bands in either the near-IR or the near-UV. However, typically beyond about $2\mu\text{m}$, the cholesteric state becomes difficult to maintain. In addition, at wavelengths shorter than about $\lambda=350\text{nm}$, many cholesteric liquid crystal components absorb or undergo photochemical changes.

4 Nano Particles and Opticules for use in Tags

4.1 A Theoretical Examination

Technological advances have made it possible to synthesize elemental and compound clusters with nanometer scale dimensions. We are particularly interested in cluster sizes in the 1-100 nm diameter range. Due to quantum size effects acting on the electrons within the clusters and the fact that visible light has wavelengths in the 400-700 nm range a variety of new phenomena have been observed. In such small clusters the number of included atoms are in the range 10-10,000. Some properties resemble those of the bulk materials while others do not. This section of the report examines the potential for developing clusters and "cluster molecules" for the purpose of optical down conversion. Ideally, we would like to design particulate material with a strong narrow absorption band in the visible-ultraviolet spectrum and have them emit the absorbed energy in a narrow near infrared band for which the atmosphere is transparent. This would correspond to wavelengths of 890nm, 1050nm, 1270nm, and 1550-1750nm.

In the laboratory it is possible to synthesize nanocrystals in solution with and without a surface passivation for optical studies. Surface properties dominate the optical response of small clusters and improperly terminated surfaces may quench luminescence. Laboratory surface passivations are unlikely to be robust against degradation, in the form of oxidation or abrasion, if removed from solution and dried. Protection against oxidation is a serious consideration given that the entire cluster is likely to be converted into an oxide. To date, there are no pure oxide clusters that luminesce in the near infrared known to the authors. However, oxides such as SiO₂ (glass) and Al₂O₃ (sapphire) can be used to encapsulate useful nanocluster materials with only small modification of the intrinsic optical response.

Encapsulated nanoclusters promise to be environmentally robust and allow one to build opticules. Opticules are agglomerations of encapsulated nanoclusters wherein the encapsulating dielectric material physically supports and separates the enclosed nanoclusters in larger assemblies. These assemblies can exhibit the crystalline structure characteristic of close packed spheres and be sintered into rigid assemblies. Thus, opticule size can be varied up to the micron range with the effect of enhancing the absorption and emission intensity with respect to individual encapsulated clusters. The literature on nanocluster research was reviewed with the intent of identifying the most promising paths to the design and synthesis of nanocluster based optical down conversion structures.

Clusters of metal particles containing n atoms ($2 \leq n \leq 1000$) have been the subject of study for several decades. The focus has been to understand the evolution of the electronic properties of an assemblage of a finite number of atoms to the pseudo-infinite bulk limit. Evolution of the electronic structure has been compared to the evolution of the nuclear shell structure of atoms as the mass increases. Clusters of semiconductors have received significant attention as quantum dots prepared in epitaxial growth systems. More recently, attention has been devoted to the synthesis of spherical semiconductor clusters by solution growth. The electronic structure of semiconductor clusters is analogous to the electronic structure of multielectron atoms. Comparing the two systems, semiconductor cluster typically demonstrate a much higher degree of structure in the allowed electronic levels. In either case, the

term "nanoclusters" is now in common use. In neither case does the use of this name bring anything new to the discussion. It simply reflects the current fascination with structures in which quantum size effects in three dimensions are important.

In the present study we consider nanocluster materials for the down conversion of visible to infrared light by a microscopic powder. Since the optical properties of bulk materials are well known, the advantages and applications of powders with particles having bulk-like optical properties are readily predictable. To achieve something out of the "ordinary" we have considered nanocluster materials. Both metallic and semiconductor nanoclusters are examined to find candidates for optical down conversion in a material that is a microscopic powder, nontoxic, and resistant to environmental degradation.

The studies of metallic and semiconducting nanoclusters represent two distinct areas of research that, historically, have not overlapped. Metal nanoclusters are conventionally prepared as beams in a vacuum and studied spectroscopically. Semiconductor nanoclusters have been prepared in epitaxial growth systems as "quantum dots", prepared via island growth methods on a semiconductor substrate. With the recent interest in preparing nanocluster by growth from solution the gap has narrowed. Both metal and semiconductor nanoclusters can be grown in solution. Further, both systems are amenable to core/shell constructions. Metal/metal, metal/dielectric, and semiconductor/semiconductor core/shell composites have been synthesized. It is believed that a core/shell structure will be required for environmental stability.

4.1.1 Semiconductor Nanoclusters

Semiconductors have been the target of most of the nanocluster work in which photoluminescence studies have been performed. Photoluminescence occurs when a material is optically excited by photons of a given wavelength and photons of a different (and usually longer) wavelength are emitted. In other words, photoluminescence is a measure of the down conversion properties of a material. Photoluminescence (PL) in semiconductors is widely exploited in the fabrication of light emitting diodes (LEDs) and solid state lasers diodes. III-V semiconductors GaAs and InP are good light emitters at wavelength in the very near infrared. Other binary III-V compounds that emit in the infrared are GaSb ($\lambda \sim 1500\text{nm}$), InAs ($\lambda \sim 3500\text{nm}$), and InSb ($\lambda \sim 6900\text{nm}$). The wavelengths given are all for the bulk solid. When quantum confinement effects become important the maximum emission wavelength decreases. If one targets emission in the relatively broad 1550-1750nm transparency band in air InAs and InSb become the III-V candidates for study. Of these two candidates, InAs is more easily synthesized and has been studied extensively both as bare nanocluster and with a wide band gap shell [13–16].

Other semiconductor materials that have been studied are the II-VI compounds with Zn, Cd, or Hg cations and S, Se, or Te anions. Many of these semiconductors are easily synthesized in solution. However, the II-VI semiconductors are more ionic than III-V semiconductors and consequently have a larger band gap. II-VI nanoclusters are exploited for the fact that they can be tailored to luminesce across the entire visible spectrum as a function of semiconductor and cluster size. Only the Zn and Cd compounds have received much experimental attention and only HgSe and HgTe have bulk band gaps sufficiently small as to

make them candidates for down conversion into the infrared. Other somewhat more remote candidates are the lead chalcogenides; PbS, PbSe, and PbTe, and the II-V compounds; ZnSb and CdSb. Most of these candidates also feature at least one toxic constituent atom.

InAs is the most promising semiconductor candidate currently available. InAs/CdSe core/shell nanoclusters with a core radius of 2.5nm luminesce at about $\lambda=1300\text{nm}$ [13]. Increasing the core radius would allow this to be shifted continuously toward the bulk limit of $\lambda=3500\text{nm}$. The shell material (ZnSe and InP shells have also been demonstrated) performs several functions. Most importantly, it provides a crystalline termination at the InAs surface. Luminescence in semiconductor nanoclusters occurs by the recombination of a photoexcited electron-hole pair. An imperfectly terminated surface offers nonradiative recombination paths as well as recombination paths which luminesce at longer than desired wavelengths [17]. These are often lumped with nonradiative paths because the researcher typically does not have the experimental capability to detect them. Second, the band gap of the shell material affects the confinement of electrons and holes within the InAs core. Thus modification of the shell material affects both the emission wavelength and quantum yield of the core luminescence. Third, the shell material acts as a buffer against the environment.

If it is essential to luminesce at wave lengths greater than that corresponding to bulk InAs (for example) it may be possible to construct what are known as type-II core/shell heterostructures [18,19]. A concrete example would be an InAs/GaSb core/shell nanocluster. The valence and conduction electron states in GaSb are both somewhat higher in energy than the corresponding states in the InAs core. When the composite is photoexcited electrons are collected in the InAs and the holes are collected in the GaSb. Although spatially separated there is significant overlap of the electron and hole wave functions at the interface and luminescent recombination occurs. However, the wavelength of the emitted light is a function of the energy separation between the lowest electron state in the InAs and the highest hole state in the GaSb. This separation will be smaller than the quantum confined band gap of either component semiconductor. The band gap is inversely proportional to the wavelength so longer wavelength emission would result.

What about silicon? Silicon nanoclusters with cleanly terminated surfaces luminesce in the visible [20]. The most efficient luminescence occurs when the particles are sufficiently small as to promote recombination at the direct band gap (blue). In larger nanoclusters the indirect gap is shifted to about 2eV (yellow). Luminescence occurs because the bulk selection rules forbidding recombination across an indirect gap break down in the quantum size effect limit. However, if Si were used as a hole accumulator in a type-II configuration with a direct band gap material to collect the electrons, efficient long wavelength luminescence might be achievable. This possibility has not been explored.

4.1.2 Metallic Nanoclusters

Until recently metal nanoclusters had not been considered as candidates for the down conversion of optical energy. Au and Ag metal nanoclusters had extensive investigation made of their optical properties in visible spectrum [21–25]. This is a consequence of the strong surface plasmon feature each metal exhibits in the visible. Conductive metallic nanoclusters are susceptible to collective oscillatory excitation of electrons at the surface of the cluster [26].

These collective excitations are plasmons and involve the entire surface of the cluster. Consequently, the resonance energy of the plasmon is strongly dependent on both the size and the shape of the cluster. To a lesser extent the plasmon resonance is dependent on the nature of the surface passivation.

Surface plasmons are of interest because of the strength of the interaction they exhibit with light. Plasmons can also store energy in a spatial extent much smaller than the wavelength of the exciting light. Plasmons can also transfer across the surface of a structure such as a nanorod and emit light at a point distant from the point of excitation [27–29]. Luminescence of metallic nanostructures at or near the plasmon resonance energy is now well documented. What has not been appreciated is that metal nanoclusters luminesce in the infrared presumably at the Highest Occupied Molecular Orbital (HOMO)-Lowest Unoccupied Molecular Orbital (LUMO) gap. This is equivalent to the band gap of a semiconductor. Infrared luminescence at the HOMO-LUMO gap in Au nanoclusters was first observed only in 2000. To a large extent the late date is attributable to the fact that no one expected to find infrared luminescence in metal nanoclusters.

At first it might seem that this should be an obvious expectation. Individual metal atoms in the vapor phase are known to luminesce and even lase under appropriate conditions. Measurements of both the ionization potential (IP) and electron affinity (EA) have been made as a function of cluster size for a number of simple and transition metals [30–45]. With increasing cluster diameter the IP and EA both tend toward the work function of the bulk metal [46, 47]. In a bulk semiconductor the IP corresponds to the level of the valence band maximum with respect to the vacuum as a reference while the EA measures the conduction band minimum with respect to the vacuum. Consequently, the difference EA-IP is a direct measure of the semiconductor band gap. A similar approximation applied to measurements of metal nanoclusters predicts a band gap of 2eV or more for small clusters. This would result in visible luminescence that is not observed. To obtain a better estimate of the optical properties requires a somewhat better model of the electronic structure of a cluster.

One approximate model of electronic structure in a metal nanocluster is the shell model [48]. It asserts that to first order the atomic structure and size of the cluster is unimportant. The electrons are confined in a perturbed harmonic potential and fill well defined shell with fixed occupation numbers. The extent to which the shell is filled depends on the total number of valence electrons in the cluster. The critical feature of this model is that there is an energy gap between shells. When one measures the electron affinity of metal clusters the dependence between cluster size and the EA is not smooth for very small cluster sizes (less than 100-200 atoms). At specific cluster sizes, as measured in numbers of atoms, there are sharp jumps in the measured EA. These are interpreted as the energy gaps between shells. The interpretation is as follows [33, 49]. For the coinage metals (Cu, Ag, Au) assume an electron configuration of $d^{10}s^1$. In this case the electron affinity is dominated by s electron shell filling, one such electron per atom. When a shell has one hole in a neutral cluster creating the negative anion fills the shell and the EA then measures the highest energy of the filled shell. Adding one atom to such a cluster fills the shell in the neutral cluster and creating the anion forces the extra electron into the next higher shell. The EA then measures the lowest energy of that normally unoccupied shell. Hence, one jump in the EA at a shell

closing corresponds roughly to a HOMO-LUMO gap in the cluster.

In Ag and Au clusters, examination of the EA versus cluster size shows evidence of shell fillings at 8, 20, 34, and 58 atoms. In Ag the jump is roughly 0.5eV ($\sim 2500\text{nm}$) and for Au the jump is roughly 1.0eV ($\sim 1200\text{nm}$) [33]. The difference is attributed to relativistic effects present in the Au clusters increasing the gap. Infrared luminescence from 28 atom Au clusters luminescence at 1.13eV ($\sim 1100\text{nm}$) is observed, in agreement with the rough estimate provided by the electron affinity data [50]. Knowing this creates some expectation that metallic clusters may be adaptable to use in the down conversion of optical energy. Au clusters are amenable to synthesis in solution and are nontoxic. While bare Au particles are expected to agglomerate and suffer from surface termination problems it has also been demonstrated that Au nanoclusters may be synthesized with SiO_2 shells [51]. This can be expected to provide reasonable protection against environmental degradation and agglomeration into large irregular metal structures.

What is not known, and is essential to efficient down conversion, is the ability of a Au/ SiO_2 core/shell nanocluster to convert energy absorbed at the plasmon resonance to emission in the infrared. The efficiency of the process is dependent both on the absorption cross-section and the pump wavelength and quantum efficiency of the luminescence. In simpler terms, what fraction of the incident photons are absorbed and what fraction of the absorbed energy gets emitted in the infrared. Both numbers should be as large as possible. Semiconductor nanocluster studies often cite quantum efficiency but not absorption efficiency. To date the very limited data for Au nanoclusters suggests a very low quantum efficiency with a very large absorption efficiency due to the plasmon resonance. However, the low quantum efficiency may simply be a reflection of a poor surface termination. SiO_2 encapsulated nanoparticles have not been tested for quantum efficiency.

Beyond the simple synthesis of Au/ SiO_2 nanoclusters the next step in complexity would be to assemble clusters of the core/shell nanoclusters. If one thinks of a nanocluster as a pseudo atom (as in the case of semiconductor nanoclusters) one could think of sintering a controlled number of Au/ SiO_2 nanoclusters into a pseudo molecule. On a grand scale, an inverse opal photonic lattice has been demonstrated using this approach [51]. The SiO_2 provide for a sinterable coating that preserves the optical properties of the embedded nanosphere of Au. For this reason it is proposed that such clusters be called opticles. There are two motivations for the construction of opticles. First, if the dielectric shells are sufficiently thin resonant coupling between the cores may be obtained, thereby enhancing the optical response [27]. Second, and independent of the possibility of resonant coupling, the size of the cluster becomes a design parameter. For a given application the size of the cluster will be an issue in the handling and dispersal of the powder. Second, this route may obtain the maximum possible core density. The alternative would be to embed the nanoclusters into a transparent support matrix that would then be powdered. The support matrix would certainly decrease the core density of the composite and further modify its optical properties.

4.1.3 Final Thoughts on Nanocluster Physics

The pursuit of Au/ SiO_2 nanoclusters seems to offer the potential for a powder medium for the efficient down conversion of visible light into the infrared. A SiO_2 shell offers substantially

better environmental protection to the core than does a semiconductor/semiconductor core shell arrangement, as the shell is prone to oxidation and chemical attack where SiO_2 is not. The SiO_2 shell is transparent to much shorter wavelengths than any of the known semiconductor shells allowing the pump wavelength to enter the near ultraviolet as well as the sintering of multiple nanoclusters into opticles and larger photonic constructs. The synthesis of Au/SiO_2 is a known process and the product is eminently non-toxic.

4.2 Laboratory Investigation of Nano Particles

The goal of the laboratory effort was to develop new nanomaterials which exhibit significant invisible (i.e. SWIR, $800\text{nm} < \lambda < 1500\text{nm}$) fluorescence when illumination by invisible sources, such as a YAG laser. The use of semiconductor nanoclusters as the tag material was motivated by the lack of efficient organic fluorophores in the SWIR region. In fact, the standard material which we and others have chosen to use to benchmark our new materials is IR-26 which has peak output at 1170nm , but reportedly less the 1.8% conversion at the optimal excitation wavelength of 770nm .

Making and characterizing SWIR emitting materials is very challenging and requires special optical set-ups and methods to detect the invisible light. The first part of this project consisted of developing the characterization capabilities. Our original intention was to use a cooled InGaAs detector specially purchased for our pre-existing SPEX fluorolog II instrument together with SWIR gratings which would have given us both detection and energy calibration of the SWIR wavelengths. However, because of supplier problems with the detector we had to alter our plans and purchased ambient condition InGaAs from NRC corporation and develop both line imaging and integrating sphere capabilities, but without the ability to energy resolve the PL spectra. On the positive side the detector has NIST traceable absolute calibration allowing the use of excitation with a laser of known power to help extract the absolute quantum efficiency (QE) of the particle fluorescence down conversion.

Figure 34 shows the line imaging capabilities our set-up. A 2:1 demagnified image of the excitation laser source (here, $\lambda_{excitation}=514\text{nm}$) and one of our invisible PbS nanocluster solutions in octane. In the foreground is the chopper which can provide a synched lock-in signal for our lock-in amplifier. In the case of the majority of our samples the signal was sufficiently strong that lock-in detection was not necessary. The cuvette holder is in the background, an achromatic imaging lens focuses the image of the PL line source in the NIST traceable detector head (foreground) which has a 600nm long-pass filter which reduces the background to $\sim 3.0\text{nW}$.

Figure 35 shows the set-up using 1060nm YAG illumination at 6mW . The Ar ion laser is used to illuminate the set-up. The integrating sphere has its calibrated InGaAs detector mounted on the far side of the sphere with a 600nm long-pass filter to block the background excitation wavelength. Separate detectors are used to measure the incident and transmitted excitation to calculate the fraction of the beam absorbed, and to estimate the QE. The sphere efficiency in the SWIR was measured by illuminating the sphere interior with the YAG laser at $\lambda=1060\text{nm}$ and measuring the power detected using the InGaAs head. Unfortunately, the measured sphere efficiency in the SWIR is only 0.2%, compared to $\sim 4\%$ in the visible so our signal to noise ratio (SNR) was not as high as hoped. However, as will be evident later in

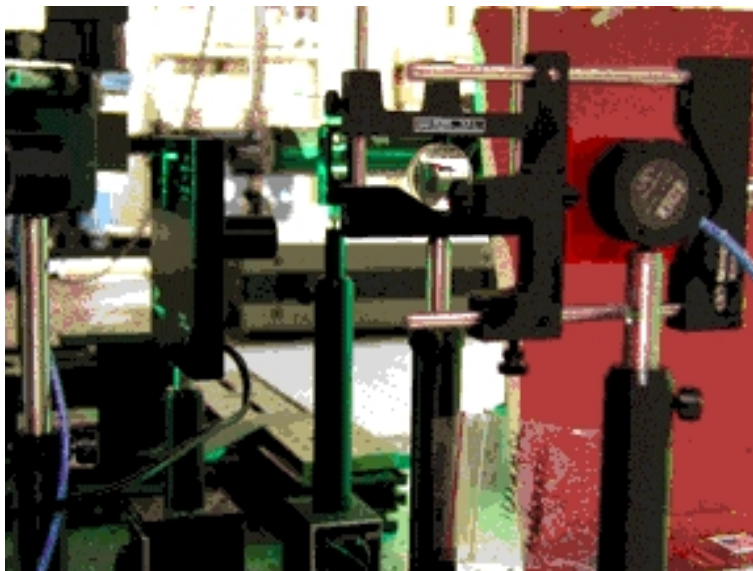


Figure 34: Set-up for laser-line PL imaging of dilute solutions of nanoclusters.

this report our best samples could be investigated using only line imaging, so this was not an issue.

Figure 36 shows the technique for measuring the total integrated light from a sample filling a square cuvette of 1cm path length and 5 optical faces. The red PL glow from the sphere is observed. In the foreground is the holder used to reproducibly insert the sphere, supported on a thin stainless steel rod into the center of the sphere. A detector for both the incident and transmitted excitation light is used to determine the fraction of excitation light absorbed. The Si or InGaAs detector head is in the sphere port on the opposite side of the sphere.

4.2.1 Nanocluster Sample Preparation

Two methods were used to prepare the visible and SWIR materials used for PL evaluation as described in the previous section. The first is the inverse micelle synthesis method originally developed and patented here at Sandia National Laboratories. The second method is a unique metathesis method most recently developed here at Sandia and applicable to a wide range of nanomaterials. Basically, non-aqueous sources of Pb(II), Cd(II), or Hg(II) (typically the corresponding nitrate, perchlorate, or chloride in THF) have a suitable stabilizing, coordinating agent added (typically a block copolymer or TOPSe) to coordinate the divalent cation source. Then a non-aqueous source of S, Se or Te (typically Li₂E, E=S, Se, Te in THF) is slowly added under Ar with vigorous stirring. The resultant clusters are then diluted to a suitable concentration (typically, 10⁻⁴M) to allow at least 50% of the excitation beam to be absorbed.

The quantum size effect and interface tuning may be used to adjust both the absorbance spectra (color) and PL of the quantum dot (Qdot). The advantage of using only small (d~2nm) Qdots and varying the material or interface is that a large Stokes shift between

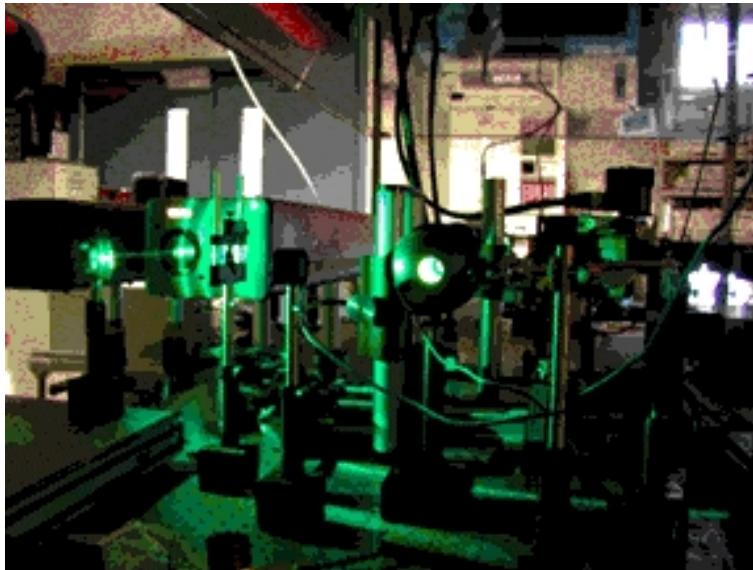


Figure 35: Set-up for SWIR PL detection using an integrating sphere.

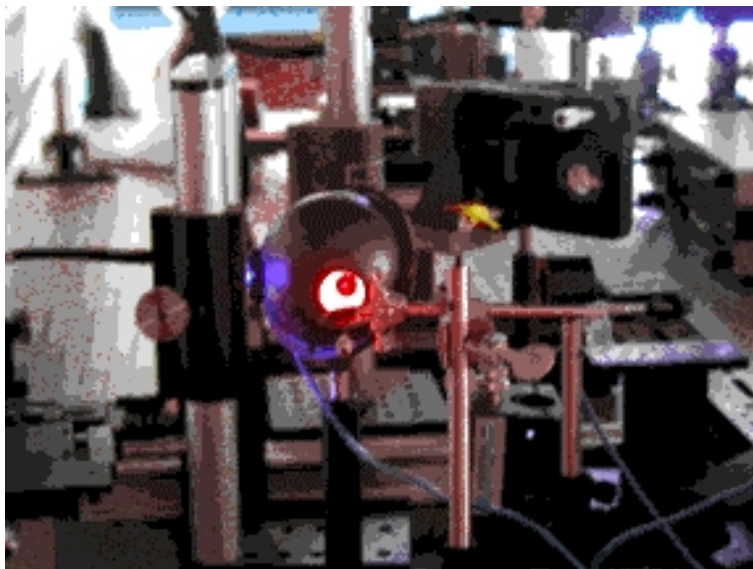


Figure 36: Set-up showing red PL from a CdS nanocluster sample illuminated with invisible, 365nm laser light and collected at a baffled detector of an integrating sphere.

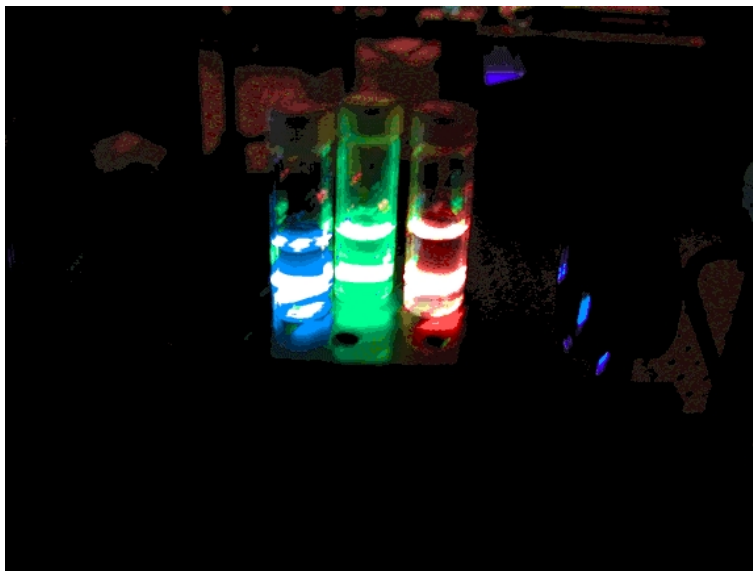


Figure 37: Invisible UV illumination, 365nm, of CdS qdots of the same size but different interface chemistry shows blue, green, and red output from the dots, with high efficiency.

absorbance and PL is achieved, analogous to a dye. Thus, interface tuning via the organic absorbed species is a desirable aspect of our synthetic procedures. An example of complete visible coverage (blue, green, and red) is shown for nanosize, $d \sim 2\text{nm}$ CdS in figure 37.

In the case of SWIR emitting nanoclusters like the dye IR-26, PbS, PbSe, HgS, and HgSe one cannot obtain pictures like Figure 37 with an ordinary camera, but must rely on a calibrated InGaAs detector as discussed in the previous section, combined with a cut-on filter which eliminates nearly all of the scattering laser excitation light.

A material like PbS which has a bulk band gap of around 0.2eV, when quantum confined properly and fully dispersed into a matrix will provide an invisible taggant as illustrated by the paper towel stained with green emitting CdSe and illuminated with a invisible source (a 365nm lamp in the foreground in this case).

4.2.2 Factors affecting NIR and IR PL efficiency

Table 5 shows the background corrected energy as measured with our NIST calibrated detector using a 600nm long-pass filter to screen out any visible light due to Rayleigh scattering. The invisible light output was compared to a moderately efficient, readily available organic dye, IR-26 in benzyl alcohol at 10^{-4}M (this was also the typical concentration of Pb or Hg in the samples). Since we could not determine the invisible spectral energy profile with our set-up we set the detector at $\lambda=1060\text{nm}$ (the peak of the IR-26 dye is known to be $\lambda=514\text{nm}$). Due to the excellent IR output of our nanocluster samples it was not necessary to use either the integrating sphere nor the chopper was required.

The best nanocluster materials prepared have over 2 orders of magnitude greater SWIR emission than IR-26. We feel that the 1.8% QE reported for IR-26 is overstated, but our low observed output may also reflect less-than-optimal pumping of the dye at $\lambda=514\text{nm}$. In any

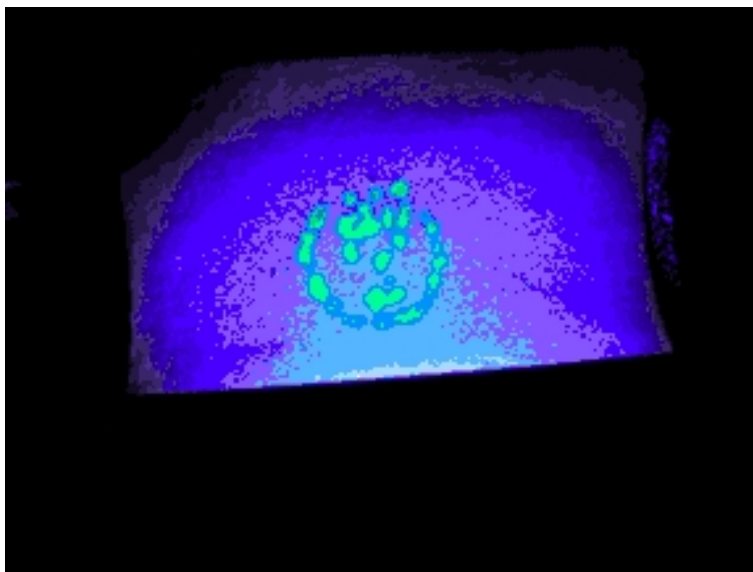


Figure 38: Invisible lamp illumination of a "nano-art-Qdot" face of CdSe (yellow in absorbance) on a paper towel glows intensely green. The Si CCD array also responds to the background ultraviolet illumination of the towel.

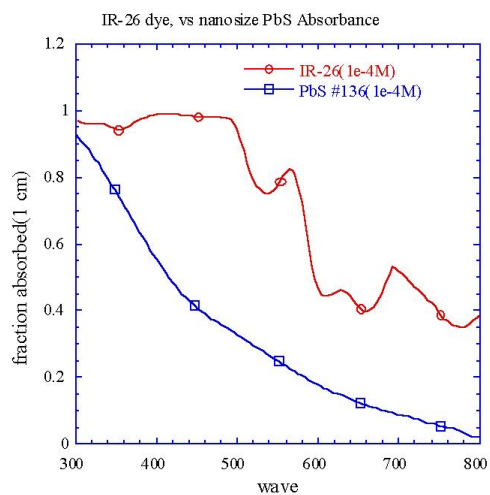


Figure 39: Absorbance spectra of nanosize PbS and the reference standard IR-26 both at 10^{-4} M. The ordinate is the fraction of the incident beam absorbed in 1cm.

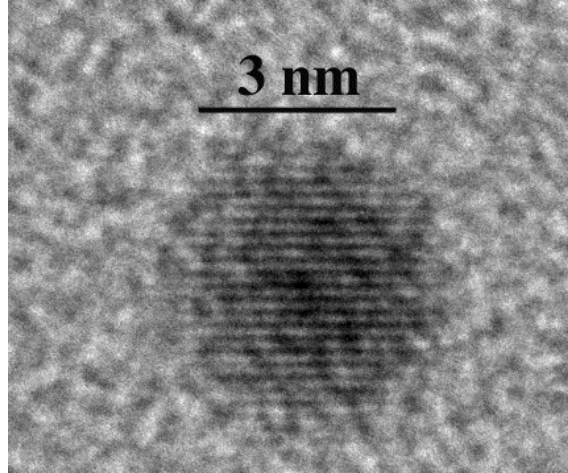


Figure 40: TEM of nanosize SWIR emitting PbS whose spectra was shown in Figure 39.

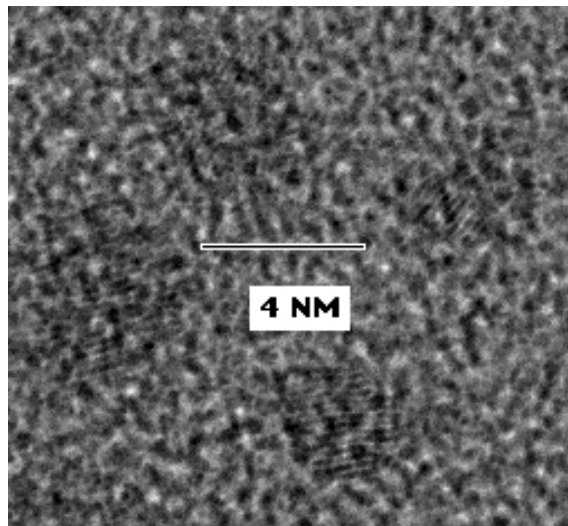


Figure 41: HRTEM of nanosize red and SWIR emitting D=3nm HgSe.

Sample	Concentration	I(90,nW)	Comment	fraction absorbed
IR-26 dye	10^{-4} M	2.8	$\lambda_{max} = 1170$ nm	0.82
DCM laser dye	10^{-6} M	36	$\lambda_{max} = 644$ nm, red	
PbSe #4/thf	10^{-4} M	0.0	no stabilizer used	0.49
PbSe/thf, Pb:Se=1:1	10^{-4} M	1.4	Stab=Poly(pyrrol) -co-c16, invisible	
PbSe #5/thf	10^{-4} M	28	Stab=TOPSe, PL=invisible	0.48
PbSe #6/c12sh/thf	10^{-4} M	100	Fresh sample, under Ar	0.42
PbSe #6/c12sh/thf	10^{-4} M	160	1 day old, under Ar	0.42
PbSe #6/c12sh/thf	10^{-4} M	149	5 days old, under Ar	0.42
PbS #67(8/94),c12e5/c8	2×10^{-4} M	43	Very old sample, Ar	0.24
PbS #100,c12e5/c8	2×10^{-3} M	0.4	Very old sample, Ar	0.42
PbS #136/c12sh/thf	10^{-4} M	760	2 days old, invisible PL	0.30
PbS #136/c12sh/thf	10^{-4} M	900	20 days old, stored in air	0.30
PbS #138/Poly(pyrrol)/thf	10^{-4} M	5.4	1 day old, invisible PL	
PbS #139/c12sh/thf	10^{-4} M	200	fresh sample, under Ar	0.31
PbS #139/c12sh/thf	10^{-4} M	380	1 day old, under Ar	0.31
PbS #139/c12sh/thf	10^{-4} M	574	7 days old, under Ar	0.31
PbS #140/c12sh/thf	10^{-4} M	92.5	fresh, Pb:S = 2:1	0.079
PbS #140/c12sh/thf	10^{-4} M	237	5 days old, Pb:S=2:1	0.079
PbS #141/c12sh/thf	10^{-4} M	217.5	5 days old, Pb:S=1:1	0.172
PbS #141/c12sh/thf	10^{-4} M	556		0.172
PbS #142/c12sh/thf	10^{-4} M	16	fresh, Pb:S=1:2	0.048
PbS #142/c12sh/thf	10^{-4} M	0.2	5 days old. Pb:S=1:2	0.048
PbS #144/AOT/c8	10^{-4} M	1.7	fresh, Pb:S=1:1	0.021
PbS #144/AOT/c8	10^{-4} M	0.0	5 days old, Pb:S=1:1	0.021
PbS #145/AOT/c8	10^{-4} M	4.1	fresh, Pb:S=1:2	
PbS #145/AOT/c8	10^{-4} M	0.0	5 days old	
HgS/c12sh/thf	10^{-4} M	0.0	fresh sample, under Ar	
HgSe #14/TOPSe/thf	10^{-4} M	1.3	1 day old, invisible PL	
HgSe #15/c12sh/thf	10^{-4} M	1.4	fresh sample, under Ar	

Table 5: Relative Q.E.s of Standard Dye vs Nanosize Semiconductors (excitation for $\lambda=514$ nm with a path length of 1cm, incident intensity was 320mW).

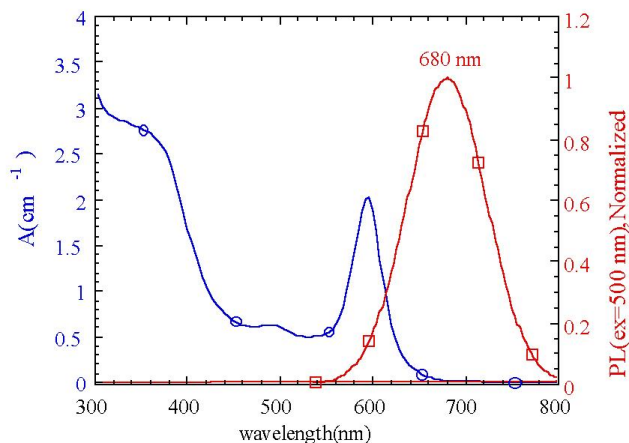


Figure 42: Absorbance and SWIR PL of HgSe in thf.

case, the goal of this LDRD, to develop highly efficient SWIR and IR emitting nanocluster materials, has been achieved. As the formulations and conditions for generating such novel emitters are of great importance to technology, the exact synthesis methods must await patent protection and will not be a part of this report. Instead we will discuss the general chemical factors which we find to be important for these new SWIR nanophosphors.

In general the controlling factors for strong NIR emission seem to be the same as we have recently demonstrated for visible nanocrystals of CdS, and CdSe, age, state of dispersion, method of surface passivation, and reaction stoichiometry.

As Table 5 shows, PbS yielded the best invisible emission, with suitable aging at room temperature increasing the yield with time. PbSe was the next best material, with HgS and HgSe quite low in output energy. Surprisingly, we discovered formulations not requiring inverse micelles which yielded exceptionally strong SWIR emission—exceeding samples made in inverse micelles like PbS #144 or PbS #67. Also, the samples could be prepared in air which was very surprising. Further, no decrease in SWIR output was observed even upon intense optical pumping using our laser excitation source and checking the sample over a period of several weeks. This bodes extremely well for applications in normal environments with moisture and air present. These results parallel our observations of properly passivated CdS samples which show no decrease in visible output over periods exceeding 3 years.

We direct the reader's attention to PbS #140, #141, #142, in which the effect of stoichiometry was studied. Obviously stoichiometry is of great importance and it is better to be Pb rich than S rich, as over time, the S rich sample, Pb #142 becomes optically dead in the SWIR. We direct attention to samples PbS #136, #139, and #141 which had the greatest SWIR emission, even when fresh. Never-the-less, over time, this output increased drastically, just as we observe for visible emission from nanosize CdS and CdSe. This appears to be a universal phenomena which is related to some type of surface reconstruction which alters the carrier recombination probability in a favorable manner. Proper aging is obviously an

important factor.

Once the sample is about 2 weeks old, even when stored in air, PbS #136, no decrease in SWIR output is observed which we find interesting. This also means practical applications of these materials as invisible taggants for various applications is very promising.

4.2.3 Future Directions

In addition to filing a patent on our process to produce these materials, we need to obtain energy resolved SWIR spectra from the various high efficiency materials which we have prepared. This requires obtaining the requisite SWIR gratings and cooled InGaAs detector for the SPEX double grating instrument. We plan on pursuing this goal because of the very good results obtained with this short program.

As a final note, months after completing the laboratory work for this project, we learned of a commercial source for IR quantum dots or IR nano-particles intended for use as fluorescent dye additives [52]. Their materials do not appear to address the exact same mission space of our particles and their efficiencies are not quite as high. Nonetheless, it is important to be aware of commercial alternatives and the range of materials offered by such companies.

5 Non Optical Tags

While this report primarily covers technologies for optical tags, during the investigation a number of non optical tagging options, either based on commercial products or simply unique technical approaches. Rather than waste the effort which accumulated this knowledge, we briefly mention the high points of what was found here.

The technologies reported here are most useful for short range (~ 100 foot) applications and include optical, RF, scent, magnetic or other remote sensing technology suitable for the purpose. A useful summary of optical and RF tags is given in [53].

5.1 Magnetic Technologies

We were unable to identify any magnetic technologies that would operate over ranges on the order of ~ 100 feet in an automated search and track manner. The most common magnetic detectors are those used in metal detectors and there are several different types of circuits for such devices all of which detectors depend on induced currents in a metallic object. Then the object can be categorized by inductance and resistive effects. Alternatively, the metal detectors in airports are reported to sense currents induced by metal objects moving through them. This, however, is still much different than a search and track function.

5.2 Chemical (Scent) Technologies

Scent is another difficult characteristic to use for search and track. Unique signatures are probably available through the use of volatile compounds such as fluorocarbons that give distinct negative ion mass spectra (most natural products give good positive ion mass spectra but relatively poor negative ion mass spectra). Nitro compound often also provide unique negative ions in a mass spectrometer and therefore explosives can be detected by this technique. However, unless the sensor is moved toward the source of the scent, it is probably much more difficult to track the source than to detect it.

DARPA has considered using insects to collect scents or chemical residues. It is again not obvious how such technologies could be used to track an object.

5.3 RF Harmonic Tags

RF tags are ubiquitous, and are frequently based on harmonic generation, but are generally close range (a few meters). However, simple, lightweight harmonic mode radar tags transmitting at 3.2cm or 917MHz (and receiving at 1.6cm or 1834MHz) have been used by researchers to track insects at ranges of 50 meter and appear to be adaptable for other applications.

Harmonic (frequency doubling) RF tags are available from many vendors for anti-theft applications, however, it is not clear how to apply these relatively large (centimeter dimension) devices to search and track problems. These systems appear to have a common architecture: a diode, generally a high speed diode such as a Schottky diode, that links two conductors. The conductors may be, for example, simple and lightweight wires, or may be

spirals etched onto a printed circuit board. At low powers this simple device generates harmonics of the incident radiation and therefore provides a relatively good signal to noise ratio. At high powers the induced currents can be sufficient to "burn out" the diode, rendering the device ineffective. This simple manner of deactivating an RF tag is useful in retail.

This approach has been carried to a remarkably small and lightweight design for use in tracking insects at ranges of tens of meters. The most complex of three reported designs was reported in Nature [54]. This design shown in this report is 16mm long with an apparently unpackaged Schottky diode in the center and a coil at one end. The total weight is 12mg and the detection range is several hundred meters. An apparently similar design uses a Schottky diode in the center of a 16mm dipole antenna with a 3nH inductor at one end [55]. The weight of this device was reported to be 3mg. Yet another group reported a longer (8cm) but lighter (0.4mg) design consisting of aluminum bonding wire attached to a low power Schottky diode [56]. The range of this device is only about 50 meters, but the transponder is about 10 times lighter than previous designs.

According to information from the Rothamsted Radar Entomology Unit website [57], the transponders are not commercially available at this time. It is not clear if they are using unpackaged diodes or if they are removing the packaging from inexpensive commercial diodes.

5.4 Other New Technologies

Another interesting new technology involves the possibility for encoding individual photons with spin angular momentum [58,59]. In addition to the angular momentum associated with circular polarization, the researchers found that they could create photons with additional orbital angular momentum. It isn't yet clear how to make materials that selectively interact with photons with orbital angular momentum. However, if this were possible, unique tags might be created.

The frequency range between long wave infrared and microwaves, the terahertz region, is under intense scrutiny as new sources and detectors become available for this part of the EM spectrum. Terahertz sensitive tags may give another unique signature.

5.5 Other Commercial Tagging Technologies

Many examples of fluorescent tags, photochromic tags, thermochromic tags, optically variable devices (pigments, holograms), and random particle tags are given. Not mentioned are electrochromic tags or electroluminescent tags - two technologies that might require contact or at least short range sensing. Other technologies including delayed fluorescence introduces the possibility of electrochromic tags [60]. There is also discussion of energy storage based tags and two photon tags, both of which are generally based on rare earth oxides and related matrices. Such tags require the absorption of at least two photons before emission occurs. This allows for an up conversion process, e.g., two infrared photons can be absorbed to give a visible light photon. Such tags may be useful as unique identifiers, and may be used for search and track with suitable sources and detectors.

6 Summary

Here we have taken a brief look at technologies for relatively short range tagging with a concentration on optical approaches. The desire was to operate at wavelengths easily sensed by low-cost commercial components, even if a custom sensing instrument had to be assembled. Technologies examined primarily covered the range of wavelengths from the UV through the SWIR. For clandestine operations, it is most desirable to operate at wavelengths outside the common detection range of the human eye and simple CCD sensors such as those in common video cameras and hand-held video cassette recorders. This requires operation either in the UV or SWIR. Most CCDs have very limited sensitivity to UV and no sensitivity to SWIR or wavelengths longer than roughly $\lambda=1\mu\text{m}$. For the latter case, fluorescent nano particles appear to show particular promise.

This work was supported by the U.S. Department of Energy under contract DE-AC04-76DP00789.

References

- [1] H. A. Smartt. Spectral tagging. M.S. Thesis, University of New Mexico, Albuquerque, NM, USA, December 2002.
- [2] Schott glass technologies. [http : //www.us.schott.com/sgt/english/index.html](http://www.us.schott.com/sgt/english/index.html), Undated.
- [3] National institute of standards. [http : //www.nist.gov](http://www.nist.gov), Undated.
- [4] S. J. Choquette, J. C. Travis, and D. L. Duewer. SRM 2035: A rare earth oxide glass for the wavelength calibration of near infrared dispersive and fourier transform spectrometers. In *Proceedings of the SPIE, Optical Diagnostic Methods for Inorganic Transmissive Materials*, volume 3425, pages 94–102, 1998.
- [5] S. J. Choquette, J. C. Travis, and C. Zhu. Development of a near infrared transmission wavelength standard.
[http : //www.cstl.nist.gov/nist839/TAR99/tar22.html](http://www.cstl.nist.gov/nist839/TAR99/tar22.html), Undated.
- [6] National Institute of Standards. SRM 2035 certificate.
[http : //patapsc.nist.gov/srmcatalog/common/view_cert.cfm?srm=2035](http://patapsc.nist.gov/srmcatalog/common/view_cert.cfm?srm=2035), Undated.
- [7] Starna glass corporation. [http : //www.starna.com/def/dwl/HL.html](http://www.starna.com/def/dwl/HL.html), Undated.
- [8] Sumita glass corporation, japan. [http : //www.sumita – opt.co.jp/](http://www.sumita-opt.co.jp/), Undated.
- [9] *Thermodynamics Research Center AP144 Hydrocarbon Project*.
- [10] Oriel corporation web site. [http : //www.oriel.com](http://www.oriel.com), Undated.
- [11] Paul C. Sadek (Burdick & Jackson). *The HPLC Solvent Guide, 2nd Edition*, 1997.
- [12] M. F. Weber, C. A. Stover, L. R. Gilbert, T. J. Nevitt, and A. J. Ouderkirck. Giant birefringent optics in multilayer polymer mirrors. *Science*, 287(5462):510–513, March 2000.
- [13] Y. Cao and U. Banin. Growth and properties of semiconductor core/shell nanocrystals with InAs cores. *Journal of the American Chemical Society*, 122(40):9692–9702, 2000.
- [14] O. Millo and D. Katz et al. Imaging and spectroscopy of artificial-atom states in core/shell nanocrystal quantum dots. *Physical Review Letters*, 86(25):5751–5754, 2001.
- [15] D. V. Talapin and S. K. Poznyak et al. Synthesis of surface-modified colloidal semiconductor nanocrystals and study of photoinduced charge separation and transport in nanocrystal-polymer composites. *Physica E*, 14(1–2):237–241, 2002.
- [16] D. V. Talapin and A. L. Rogach et al. Dynamic distribution of growth rates within the ensembles of colloidal II-VI and III-V semiconductor nanocrystals as a factor governing their photoluminescence efficiency. *Journal of the American Chemical Society*, 124(20):5782–5790, 2002.

- [17] L. Liu and C. S. Jayanthi et al. Factors responsible for the stability and the existence of a clean energy gap of a silicon nanocluster. *Journal of Applied Physics*, 90(8):4143–4151, 2001.
- [18] D. A. Broido and K. Kempa et al. Far infrared response of InAs-GaSb type-II quantum dots. *Physica E*, 6(1–4):466–469, 2000.
- [19] A. Shik and H. Ruda et al. Non-equilibrium carriers and recombination phenomena in type-II quantum dots. *Nanotechnology*, 12(4):523–528, 2001.
- [20] J. P. Wilcoxon and G. A. Samara. Tailorable, visible light emission from silicon nanocrystals. *Applied Physics Letters*, 74(21):3164–3166, 1999.
- [21] O. D. Habermen and S. C. Chung et al. From clusters to bulk: A relativistic density functional investigation on a series of gold clusters Au_n , $n = 6, \dots, 147$. *Journal of Chemical Physics*, 106(12):5189–5201, 1997.
- [22] V. Kasperovich and V. V. Kresin. Ultraviolet photoabsorption spectra of silver and gold nanoclusters. *Philosophical Magazine B*, 78(4):385–396, 1998.
- [23] B. Preval and B. Palpant et al. Comparative analysis of optical properties of gold and silver clusters embedded in an alumina matrix. *NanoStructured Materials*, 12(1–4 part A/SISI):307–310, 1999.
- [24] J. Zhao and Y. Luo et al. Tight-binding study of structural and electronic properties of silver clusters. *European Physical Journal D*, 14(3):309–316, 2001.
- [25] T. Pham and J. B. Jackson et al. Preparation and characterization of gold nanoshells coated with self-assembled monolayers. *Langmuir*, 18(12):4915–4920, 2002.
- [26] F. Stietz and T. F. Surface plasmons in nanoclusters: elementary electronic excitations and their applications. *Philosophical Magazine B*, 79(9):1281–1298, 1999.
- [27] M. Quinten and A. Leitner et al. Electromagnetic energy transport via linear chains of silver nanoparticles. *Optics Letters*, 23(17):1331–1333, 1998.
- [28] M. L. Brongersma and J. W. Hartman et al. Electromagnetic energy transfer and switching in nanoparticle chain arrays below the diffraction limit. *Physical Review B*, 62(24):16356–16359, 2000.
- [29] R. M. Dickson and L. A. Lyon. Unidirectional plasmon propagation in metallic nanowires. *Journal of Physical Chemistry B*, 104(26):6095–6098, 2000.
- [30] M. B. Knickelbein and S. Yang. Photoionization studies of niobium clusters: ionization potentials for Nb_2 - Nb_{76} . *Journal of Chemical Physics*, 93(8):5760–5767, 1990.
- [31] M. B. Knickelbein and S. Yang. Near-threshold photoionization of nickel clusters: Ionization potentials for Ni_3 to Ni_{90} . *Journal of Chemical Physics*, 93(1):94–104, 1990.

- [32] S. Yang and M. B. Knickelbein. Photoionization studies of transition metal clusters: Ionization potentials for Fe_n and Co_n . *Journal of Chemical Physics*, 93(3):1533–1539, 1990.
- [33] K. J. Taylor and C. L. Pettiette-Hall et al. Ultraviolet photoelectron spectra of coinage metal clusters. *Journal of Chemical Physics*, 96(4):3310–3329, 1992.
- [34] M. B. Knickelbein. Photoionization spectroscopy of yttrium clusters: Ionization potentials for Y_n and Y_nO ($n=2-31$). *Journal of Chemical Physics*, 102(1):1–5, 1995.
- [35] H. Wu and S. R. Desai et al. Electronic structure of small titanium clusters: Emergence and evolution of the 3d band. *Physical Review Letters*, 76(2):2212–2215, 1996.
- [36] H. Wu and S. R. Desai et al. Evolution of the electronic structure of small vanadium clusters from molecular to bulklike. *Physical Review Letters*, 77(12):2436–2439, 1996.
- [37] G. M. Koretsky and M. B. Knickelbein. Photoionization studies of manganese clusters: Ionization potentials for Mn_7 to Mn_{64} . *Journal of Chemical Physics*, 106(23):9810–9814, 1997.
- [38] L. S. Wang and H. Wu et al. Photoelectron spectroscopy of small chromium clusters: Observation of even-odd alternations and theoretical interpretations. *Physical Review B*, 55(19):12884–12887, 1997.
- [39] G. M. Koretsky and M. B. Knickelbein. The evolution of the electronic structure in lanthanide metal clusters: Threshold photoionization spectra of Ce_n and Pr_n . *European Physical Journal D*, 2(3):273–278, 1998.
- [40] M. B. Knickelbein. The spectroscopy and photophysics of isolated transition-metal clusters. *Philosophical Magazine B*, 79(9):1379–1400, 1999.
- [41] G. H. Lee and S. H. Huh et al. Photoelectron spectra of small nanophase W metal cluster anions. *Chemical Physics Letters*, 299:309–314, 1999.
- [42] Y. Negishi and H. Kawamata et al. Photoelectron spectroscopy of tin and lead cluster anions: application of halogen-doping method. *Journal of Electron Spectroscopy*, 106(2–3):117–125, 2000.
- [43] L. S. Wang and X. Li et al. Probing the electronic structure of iron clusters using photoelectron spectroscopy. *Chemical Physics*, 262(1/SISI):53–63, 2000.
- [44] A. Pramann and K. Rademann. Size dependent evolution of the electronic structure of small rhenium clusters investigated by photoelectron spectroscopy: approaching the bulk. *Chemical Physics Letters*, 347(1–3):46–50, 2001.
- [45] K. Wong and V. Kasperovich et al. Photo-ionization efficiency curves of alkali nanoclusters in a beam and determination of metal work functions. *Applied Physics B*, 73:407–410, 2001.

- [46] E. Engel and J. P. Perdew. Theory of metallic clusters: Asymptotic size dependence of electronic properties. *Physical Review B*, 43(2):1331–1337, 1991.
- [47] M. Seidl and K. H. Meiwes-Broder et al. Finite-size effects in ionization potentials and electron affinities of metal clusters. *Journal of Chemical Physics*, 95(2):1295–1303, 1991.
- [48] K. Clemenger. Spherical supershells in metal clusters and the transition to protocrystalline structure. *Physical Review B*, 44(23):12991–13001, 1991.
- [49] B. A. Collings and K. Athanassenas et al. Optical absorption spectra of Au₇, Au₉, Au₁₁, and Au₁₃, and their cations: Gold clusters with 6, 7, 8, 9, 10, 11, 12, and 13 s-electrons. *Journal of Chemical Physics*, 101(5):3506–3513, 1994.
- [50] S. Link and A. Beeby et al. Visible to infrared luminescence from a 28-atom gold cluster. *Journal of Physical Chemistry B*, 106(13):3410–3415, 2002.
- [51] D. Wang and V. Salgueirino-Maceira et al. Gold-silica inverse opals by colloidal crystal templating. *Advanced Materials*, 14(12):908–912, 2002.
- [52] Evident technologies web site. [http : //www.evidenttech.com](http://www.evidenttech.com), Undated.
- [53] R. W. Want. Xerox corporation web site. [http : //www.parc.xerox.com/want](http://www.parc.xerox.com/want), Undated.
- [54] J. R. Riley et al. Ontogeny of orientation flight in the honeybee revealed by harmonic radar. *Nature*, 403(6769):537–540, February 2000.
- [55] J. Riley et al. Tracking bees with harmonic radar. *Nature*, 379:29–30, 1996.
- [56] J. Rowland et al. Even smaller radar tags on insects. *Nature*, 381:120, 1996.
- [57] Rothamsted radar entomology unit.
[http : //www.dysonperrins.worcs.sch.uk/Pupils/Year%2013/Jo's%20Project/homepage.htm](http://www.dysonperrins.worcs.sch.uk/Pupils/Year%2013/Jo's%20Project/homepage.htm), Undated.
- [58] J. Leach, M. J. Padgett, S. M. Barnett, S. Franke-Arnold, and J. Courtial.
- [59] Andrew Watson. New twist could pack photons with data. *Science*, 296(5577):2316–2317, January 2002.
- [60] Rudolph. L. van Rensselaer. *Optical Document Security*. Artech House, Inc., December 1993.

Distribution

1 Dr. Paul A. Cahill
10440 Stream Park Ct
Dayton OH, 45458

2 MS 1209 J. B. Woodard, 5922
1 0972 C. A. Boye, 5710
1 1202 A. N. Campbell, 5911
2 0188 H. R. Westerich, 1011
1 1206 V. L. Behr, 5932
1 0574 R. C. Ghormley II, 5902
5 1217 M. R. Ackermann, 5922
1 1217 F. T. Mendenhall, 5902
1 1361 H. A. Smartt, 5323
1 1202 M. E. Warren, 5911
1 1202 T. J. Drummond, 5911
2 1421 J. P. Wilcoxon, 1122
1 0769 R. W. Moya, 5800
1 1205 D. J. Allen, 5900

1 9018 Central Technical Files, 8945-1
2 0899 Technical Library, 9616